



44 Johnson (HHJ) method, originally developed for the surface Kirchhoff plate equation  
 45 in [39], as a post-processing scheme to approximate the surface Hessian of a scalar  
 46 function. Furthermore, we show that this scheme can be used to approximate the  
 47 *full shape operator* of the surface, which is our main goal. For closed, *piecewise*  
 48 *linear* surface triangulations, the method yields an approximation that is *provably*  
 49 *first-order* accurate in the  $L^2$  norm, i.e.  $O(h)$  where  $h$  is the maximum diameter of  
 50 mesh elements. For surfaces with boundary, some additional information is needed  
 51 at the boundary, otherwise the accuracy degrades to  $O(h^{1/2})$  near the boundary.  
 52 The method essentially consists of a matrix-vector product that computes a non-  
 53 conforming surface Hessian of the mesh coordinates, followed by an  $L^2$ -like projection  
 54 to an HHJ element. The method also generalizes to higher order triangulations, with  
 55  $O(h^m)$  accuracy, where  $m$  is the polynomial degree of the triangulation. To the best  
 56 of our knowledge, no other finite element method can do this. Moreover, the lowest  
 57 order version of the method is simple to implement. Given an approximation of the  
 58 shape operator, it is then trivial to compute the principle curvatures and principle  
 59 directions of the surface.

60 Section 2 gives the basic background for working on surfaces. In section 3, we  
 61 describe a nonconforming formulation for approximating the surface Hessian of a  
 62 scalar function by an  $L^2$  like projection, and discuss the tools for dealing with curved,  
 63 parametric surface approximations. In particular, Theorem 3.5 is a crucial extension  
 64 of [39, Thm. 4.8]. Section 4 gives the finite element scheme for the  $L^2$  projection of the  
 65 surface Hessian and performs the main error analysis that includes the geometric error  
 66 of the surface approximation. Next, we describe our scheme for approximating the  
 67 shape operator of the exact surface in section 5, which utilizes an important identity  
 68 in Proposition 5.1, and discuss the details of its practical computation. Section 6  
 69 presents several numerical results illustrating the method on surfaces with and without  
 70 boundary. We close with some remarks in section 7. The supplementary material  
 71 provides an overview of essential differential geometry concepts.

## 72 2. A Surface FEM for the Surface Hessian.

73 **2.1. Surface Definitions.** Let  $\Gamma$  be a  $C^{k+1}$  connected, 2-dimensional manifold  
 74 embedded in  $\mathbb{R}^3$ , where  $k \geq 1$ . If  $\Gamma$  has a boundary  $\partial\Gamma := \Sigma$ , we assume  $\Sigma$  is piecewise  
 75  $C^{k+1}$  with a finite number of corners, with interior angle  $\alpha_i \in (0, 2\pi]$  of the  $i$ th corner  
 76 measured with respect to the Euclidean metric in  $\mathbb{R}^3$  (see Figure 1). In particular,  
 77  $\Sigma$  is globally continuous and parameterized by a piecewise curve. In addition, we  
 78 assume  $\Sigma = \overline{\Sigma_c} \cup \overline{\Sigma_s}$  partitions into two mutually disjoint, one dimensional open sets  
 79  $\Sigma_c$  (clamped) and  $\Sigma_s$  (simply supported); either set can be empty.

80 We note some facts from section SM2. Let  $\text{id}_\Gamma : \Gamma \rightarrow \Gamma$  be the identity map, i.e.  
 81  $\mathbf{x} = \text{id}_\Gamma(\mathbf{x})$  for all  $\mathbf{x} \in \Gamma$ , and let  $\boldsymbol{\nu} : \Gamma \rightarrow \mathbb{R}^3$  be the (locally defined) unit normal  
 82 vector of  $\Gamma$ . The tangent space projection  $\mathbf{P} : \mathbb{R}^3 \rightarrow \mathbb{R}^3$ , defined on  $\Gamma$ , is given by  
 83  $\mathbf{P} = \mathbf{I} - \boldsymbol{\nu} \otimes \boldsymbol{\nu}$  (see (SM2.1)), and satisfies the identity  $\nabla_\Gamma \text{id}_\Gamma = \mathbf{P}$  (see subsection 2.2  
 84 for  $\nabla_\Gamma$ ). Given a vector  $\mathbf{v} \in \mathbb{R}^3$ , it is in the tangent space  $T_{\mathbf{x}}(\Gamma)$  if  $\mathbf{P}(\mathbf{x})\mathbf{v} = \mathbf{0}$ .  
 85 We define the tangent bundle:  $T(\Gamma) = \{(\mathbf{x}, \mathbf{v}) \mid \mathbf{x} \in \Gamma, \mathbf{v}(\mathbf{x}) \in T_{\mathbf{x}}(\Gamma)\}$ . So, we say  
 86  $\mathbf{v} \in T(\Gamma)$  if  $\mathbf{v}(\mathbf{x}) \in T_{\mathbf{x}}(\Gamma)$  for every  $\mathbf{x} \in \Gamma$ ; in this case, we write  $\mathbf{v} : \Gamma \rightarrow T(\Gamma)$ .

87 Next, let  $\mathbb{R}^{3 \times 3}$  be the space of (extrinsic) 2-tensors in three dimensions, and define  
 88 the subset of tensors on the tangent bundle of  $\Gamma$ :

$$89 \quad (2.1) \quad \mathbf{T} \equiv \mathbf{T}(\Gamma) := \{\boldsymbol{\varphi} : \Gamma \rightarrow \mathbb{R}^{3 \times 3} \mid \mathbf{P}\boldsymbol{\varphi} \equiv \boldsymbol{\varphi}, \mathbf{P}\boldsymbol{\varphi}^T \equiv \boldsymbol{\varphi}^T\},$$

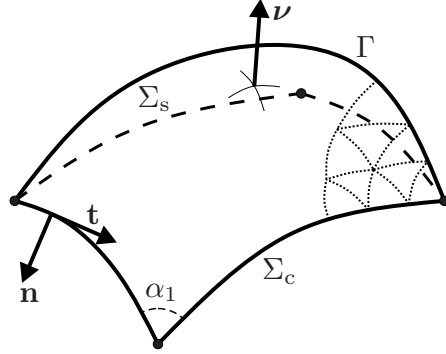


FIG. 1. Illustration of curved surface  $\Gamma$  in  $\mathbb{R}^3$  with mesh. The boundary  $\Sigma \equiv \partial\Gamma$  decomposes as  $\Sigma = \overline{\Sigma_c} \cup \overline{\Sigma_s}$  and has a finite number of corners with interior angles  $\alpha_i$ . The boundary  $\Sigma$  has (outer) conormal vector,  $\mathbf{n}$ , and oriented unit tangent vector,  $\mathbf{t}$ . The normal vector of  $\Gamma$  is  $\mathbf{v}$ . Part of the exact, curved surface triangulation  $\mathcal{T}_h$  is shown with dotted curves.

90 and define the set of symmetric tensors on the tangent bundle of  $\Gamma$ :

$$91 \quad (2.2) \quad \mathbf{S} \equiv \mathbf{S}(\Gamma) := \{\varphi \in \mathbf{T}(\Gamma) \mid \varphi = \varphi^T\}.$$

92 **2.2. Differential Operators on Surfaces.** Let  $v : \Gamma \rightarrow \mathbb{R}$  be a smooth function  
 93 defined on  $\Gamma$ . We call  $\nabla_\Gamma v \equiv \text{grad}_\Gamma v : \Gamma \rightarrow T(\Gamma)$  the surface gradient of  $v$  (see  
 94 (SM2.2)) and  $\nabla_\Gamma \nabla_\Gamma w \equiv \text{hess}_\Gamma w : \Gamma \rightarrow \mathbf{S}(\Gamma)$  the surface Hessian of  $w$  (see (SM2.3)).  
 95 Moreover, we have the function space  $L^2(\Gamma) := \{v : \Gamma \rightarrow \mathbb{R} \mid \int_\Gamma |v|^2 dS < \infty\}$ , with  
 96 inner product  $(w, v)_{L^2(\Gamma)} := \int_\Gamma wv dS$  and norm  $\|v\|_{L^2(\Gamma)}^2 := (v, v)_{L^2(\Gamma)}$ , as well as the  
 97 Sobolev (Hilbert) spaces  $H^1(\Gamma) := \{v \in L^2(\Gamma) \mid \|\nabla_\Gamma v\|_{L^2(\Gamma)} < \infty\}$  and  $H^2(\Gamma) :=$   
 98  $\{v \in H^1(\Gamma) \mid \|\nabla_\Gamma \nabla_\Gamma v\|_{L^2(\Gamma)} < \infty\}$ , with inner products given by

$$99 \quad (2.3) \quad (w, v)_{H^1(\Gamma)} := \int_\Gamma wv + \nabla_\Gamma w \cdot \nabla_\Gamma v dS,$$

$$(w, v)_{H^2(\Gamma)} := (w, v)_{H^1(\Gamma)} + \int_\Gamma \nabla_\Gamma \nabla_\Gamma w : \nabla_\Gamma \nabla_\Gamma v dS,$$

100 and corresponding norms  $\|v\|_{H^1(\Gamma)}^2 := (v, v)_{H^1(\Gamma)}$ ,  $\|v\|_{H^2(\Gamma)}^2 := (v, v)_{H^2(\Gamma)}$ . Other  
 101 types of Sobolev spaces are defined in an analogous way.

102 We denote by  $\dot{H}^\ell(\Gamma) \subset H^\ell(\Gamma)$  the Sobolev space with vanishing boundary condi-  
 103 tions up to degree  $\ell - 1$ . We will need the following subspace of  $H^2(\Gamma)$ :

$$104 \quad (2.4) \quad \mathcal{W}(\Gamma) := \{w \in H^2(\Gamma) \mid w = 0, \text{ on } \Sigma, \mathbf{n} \cdot \nabla_\Gamma w = 0, \text{ on } \Sigma_c\}, \text{ if } \Sigma \neq \emptyset,$$

105 and  $\mathcal{W}(\Gamma) = H^2(\Gamma)$  when  $\Sigma = \emptyset$ . In addition, we have  $\mathcal{V}(\Gamma) := L^2(\Gamma; \mathbf{S}(\Gamma))$ .

106 **2.3. Projection of the Surface Hessian.** Given  $w \in \mathcal{W}$ , we seek to find  $\sigma \in \mathcal{V}$   
 107 such that

$$108 \quad (2.5) \quad (\sigma, \tau)_{L^2(\Gamma)} = (\nabla_\Gamma \nabla_\Gamma w, \tau)_{L^2(\Gamma)}, \quad \text{for all } \tau \in \mathcal{V},$$

109 i.e.  $\sigma$  is the  $L^2$  projection of  $\nabla_\Gamma \nabla_\Gamma w$ , which means  $\sigma = \nabla_\Gamma \nabla_\Gamma w$  a.e. in  $\Gamma$ . The  
 110 presence of vanishing boundary conditions in  $\mathcal{W}$  is not critical; one can pose (2.5) for  
 111 any  $w \in H^2(\Gamma)$ . However, the method we develop handles the slope condition in (2.4)  
 112 as a *natural* condition, so we keep (2.5) as stated. In subsection 3.4, we show how to  
 113 handle inhomogeneous boundary conditions.

114 **3. Nonconforming Formulation of the Surface Hessian.** Major difficulties  
 115 arise in solving (2.5) if the surface is only continuous, piecewise smooth, as well as  
 116 when the data  $w$  is only a discrete, finite element function. In order to circumvent  
 117 these difficulties, and obtain a convergent approximation of the surface Hessian of a  
 118 discrete function  $w$  posed on a discrete surface, we adopt a non-conforming approach  
 119 that is first built on a mesh-dependent version of  $H^2(\Gamma)$ . This then leads to the surface  
 120 version of the Hellan–Herrmann–Johnson (HHJ) element (see [39]), which is used to  
 121 approximate the  $\sigma$  variable in (2.5). See also [10, 5, 4, 8, 3] for analysis of the classic  
 122 HHJ element. The initial idea is to triangulate  $\Gamma$  and define infinite dimensional,  
 123 mesh-dependent spaces on that triangulation.

124 **3.1. Curved Triangulations.** We start with a conforming, shape-regular, piece-  
 125 wise linear triangulation  $\mathcal{T}_h^1 = \{T^1\}$  of a polyhedral domain  $\Gamma^1$  that interpolates  $\Gamma$  at  
 126 the vertices; furthermore, the boundary vertices of  $\Gamma^1$  (namely  $\Sigma^1$ ) lie on the bound-  
 127 ary of  $\Gamma$ . See [13, 12, 17, 15, 39] for more discussion on how this triangulation can be  
 128 generated. Let  $\mathcal{T}_{\partial,h}^1$  be the set of triangles with one side on  $\Sigma^1$  and, for convenience,  
 129 assume the triangulation satisfies the following technical property (see [39]).

130 **PROPERTY 1.** *Each triangle in  $\mathcal{T}_h^1$  has at most two vertices on the boundary and*  
 131 *so has at most one edge contained in  $\Sigma^1$ .*

132 We assume  $\mathcal{T}_h^1$  is homeomorphic to an exact triangulation  $\mathcal{T}_h = \{T\}$  of  $\Gamma$ . Specif-  
 133 ically, we assume there exists a homeomorphic mapping  $\mathbf{F} : \Gamma^1 \rightarrow \Gamma$ , such that  
 134  $\mathbf{F}_T \equiv \mathbf{F}|_{T^1}$  is a diffeomorphism from  $T^1 \in \mathcal{T}_h^1$  to an exact (curved) triangle  $T \in \mathcal{T}_h$ .  
 135 Moreover, we can generate higher order approximations  $\Gamma^m$  of  $\Gamma$  by simply inter-  
 136 polating  $\mathbf{F}$  over  $\Gamma^1$  with degree  $m$  Lagrange polynomials, i.e. we have the map  
 137  $\mathbf{F}^m : \Gamma^1 \rightarrow \Gamma^m$  given by  $\mathbf{F}^m := \mathcal{I}_h^{1,m} \mathbf{F}$ , where  $\mathcal{I}_h^{1,m}$  is the Lagrange interpolation  
 138 operator of degree  $m$  given in subsection 4.1, or the standard nodal interpolant can  
 139 be used. Note that  $\mathbf{F}_T^1 \equiv \text{id}_{T^1}$ .

140 We also have maps between approximate domains, of degrees  $l$  and  $m$  by

$$141 \quad (3.1) \quad \Phi^{lm}|_T = \Phi_T^{lm} : T^l \rightarrow T^m, \text{ where } \Phi_T^{lm} := \mathbf{F}_T^m \circ (\mathbf{F}_T^l)^{-1}, \text{ so } \Phi_T^{1m} \equiv \mathbf{F}_T^m.$$

142 We also require a map from the approximate domain  $\Gamma^m$  to the exact domain  $\Gamma$ .  
 143 Specifically, given a triangle  $T^m \in \mathcal{T}_h^m$ , we define a diffeomorphism  $\Psi_T^m : T^m \rightarrow T \in$   
 144  $\mathcal{T}_h$  by  $\Psi_T^m := \mathbf{F}_T \circ (\mathbf{F}_T^m)^{-1}$ , so then  $\mathcal{T}_h \equiv \{\Psi_T^m(T^m)\}_{T^m \in \mathcal{T}_h^m}$ . The  $\Psi_T^m$  may be pieced  
 145 together to give a global map  $\Psi^m : \Gamma^m \rightarrow \Gamma$ .

146 The notation  $\Gamma$  and  $\Gamma^m$  is inconvenient because the exact domain has no su-  
 147 perscript, but the polynomial approximation does. Thus, for convenience in later  
 148 statements, we will abuse notation and make the identification  $\Gamma^\infty \equiv \Gamma$ ,  $\mathcal{T}_h^\infty \equiv \mathcal{T}_h$ ,  
 149  $\Phi^{l\infty} \equiv \Psi^l$ ,  $\mathbf{F}_T^\infty \equiv \mathbf{F}_T^l$ , etc. This is motivated by the fact that for most  $C^\infty$  surfaces  $\Gamma$ ,  
 150 the polynomial approximate domain  $\Gamma^m$ , with triangulation  $\mathcal{T}_h^m$ , would converge to  
 151  $\Gamma$  as  $m \rightarrow \infty$  with  $h$  fixed. Of course, we do not claim (in general) that  $\Gamma^m$  converges  
 152  $\Gamma$ , for fixed  $h$ , as  $m \rightarrow \infty$ , especially when  $\Gamma$  is not  $C^\infty$ .

153 Thus,  $\mathcal{T}_h^m$  is a conforming, shape regular triangulation that approximates  $\Gamma$  by  
 154  $\Gamma^m := \bigcup_{T^m \in \mathcal{T}_h^m} \overline{T^m}$ , for all  $m \geq 1$  (where  $\overline{G}$  is the closure of the set  $G$ ). Next, we  
 155 have the *skeleton* of the mesh, i.e. the set of (curved) mesh edges  $\mathcal{E}_h^m := \partial\mathcal{T}_h^m$ . Let  
 156  $\mathcal{E}_{\partial,h}^m \subset \mathcal{E}_h^m$  denote the subset of edges that are contained in the boundary  $\Sigma^m = \partial\Gamma^m$   
 157 and respect the boundary partition of  $\Sigma^m$ . The internal edges are given by  $\mathcal{E}_{0,h}^m :=$   
 158  $\mathcal{E}_h^m \setminus \mathcal{E}_{\partial,h}^m$ . We assume the meshes are quasi-uniform and shape regular [11], with mesh  
 159 size  $h := \max_T h_T$ , where  $h_T := \text{diam}(T)$  for any  $T \in \mathcal{T}_h$ . We also assume the corners  
 160 of  $\Sigma$  are captured by vertices of the mesh.

161 The main approximation properties for these maps are summarized in the next  
162 theorem (see [39, Thm. 4.1]).

163 **THEOREM 3.1.** *Suppose  $\Gamma$  is a  $C^{k+1}$  surface for some fixed  $k \geq 1$  (see [1, Para-*  
164 *graph 4.10]). Then, for all  $1 \leq l \leq m \leq k$  and  $m = \infty$  (see notation above), the maps*  
165  *$\mathbf{F}_T^m, \mathbf{F}_T^l$  described above satisfy*

$$\begin{aligned} & \|\nabla_{T^1}^s(\mathbf{F}_T^l - \text{id}_{T^1})\|_{L^\infty(T^1)} \leq Ch^{2-s}, \quad \text{for } s = 0, 1, 2, \\ (3.2) \quad & \|\nabla_{T^1}^s(\mathbf{F}_T^m - \mathbf{F}_T^l)\|_{L^\infty(T^1)} \leq Ch^{l+1-s}, \quad \text{for } 0 \leq s \leq l+1, \\ & 1 - Ch \leq \|[\nabla_{T^1} \mathbf{F}_T^l]^{-1}\|_{L^\infty(T^1)} \leq 1 + Ch, \quad \|[\nabla_{T^1} \mathbf{F}_T^l]^{-1} - \mathbf{I}\|_{L^\infty(T^1)} \leq Ch, \end{aligned}$$

167 where all constants depend on the  $C^{l+1}$  norm of  $\Gamma$ .

168 Next, recall the tangent  $\mathbf{t}$ , co-normal  $\mathbf{n}$ , and surface normal vectors  $\boldsymbol{\nu}$  from Fig-  
169 ure 1 and let  $\tilde{\cdot}, \hat{\cdot}$ , or  $\bar{\cdot}$  denote quantities defined on  $T^s$ , or using  $\mathbf{F}_T^s$ , for  $s = m, l$ ,  
170 or 1, respectively; e.g.  $\tilde{\boldsymbol{\nu}}$  is the surface normal of  $T^m$ . Then, the following estimate  
171 holds:

$$(3.3) \quad \begin{aligned} & \|\tilde{\mathbf{t}} \circ \mathbf{F}_T^m - \hat{\mathbf{t}} \circ \mathbf{F}_T^l\|_{L^\infty(T^1)} + \|\tilde{\mathbf{n}} \circ \mathbf{F}_T^m - \hat{\mathbf{n}} \circ \mathbf{F}_T^l\|_{L^\infty(T^1)} \\ & + \|\tilde{\boldsymbol{\nu}} \circ \mathbf{F}_T^m - \hat{\boldsymbol{\nu}} \circ \mathbf{F}_T^l\|_{L^\infty(T^1)} \leq Ch^l. \end{aligned}$$

173 **3.2. Skeleton Spaces.** The spaces in this section are infinite dimensional, but  
174 “mesh dependent” (see [39]), and were originally motivated by [5, pg. 1043] and [3,  
175 eqn. (2.11)]. In defining the spaces and norms, we only consider the exact triangula-  
176 tion  $\mathcal{T}_h$ , but everything generalizes to the polynomial triangulations  $\mathcal{T}_h^m$  in the obvious  
177 way. We make use of standard dG notation for writing inner products and norms over  
178 the triangulation, e.g.  $(f, g)_{\mathcal{T}_h} := \sum_{T \in \mathcal{T}_h} (f, g)_T$ ,  $\|f\|_{L^p(\mathcal{T}_h)}^p := \sum_{T \in \mathcal{T}_h} \|f\|_{L^p(T)}^p$ , etc.

179 A mesh-dependent version of  $H^2(\Gamma)$  is given by

$$(3.4) \quad H_h^2(\Gamma) := \{v \in H^1(\Gamma) \mid v|_T \in H^2(T), \text{ for } T \in \mathcal{T}_h\},$$

181 with the following semi-norm

$$(3.5) \quad \|v\|_{2,h}^2 := \|\nabla_\Gamma \nabla_\Gamma v\|_{L^2(\mathcal{E}_h)}^2 + h^{-1} \|[\mathbf{n} \cdot \nabla_\Gamma v]\|_{L^2(\mathcal{E}_{0,h})}^2 + h^{-1} \|[\mathbf{n} \cdot \nabla_\Gamma v]\|_{L^2(\Sigma_c)}^2,$$

183 where  $[[\eta]]$  is the jump in quantity  $\eta$  across mesh edge  $E$ , and  $\mathbf{n}$  is the unit co-normal  
184 on  $E \in \mathcal{E}_h$ . Hence, if the edge  $E$  is shared by two triangles  $T_1$  and  $T_2$  with outward  
185 co-normals  $\mathbf{n}_1$  and  $\mathbf{n}_2$ , then  $[[\mathbf{n} \cdot \nabla_\Gamma v]] = \mathbf{n}_1 \cdot \nabla_\Gamma v|_{T_1} + \mathbf{n}_2 \cdot \nabla_\Gamma v|_{T_2}$  on  $E$ . For  $E$   
186 a boundary edge, we set  $[[\eta]] = \eta|_E$ . We note the following norm equivalence when  
187 mapping between domains  $\Gamma^m$  and  $\Gamma^l$  [39, eqn. (4.9)]. Let  $u \in H_h^2(\Gamma^m)$  and define  
188  $\hat{u} = u \circ \Phi^{lm} \in H_h^2(\Gamma^l)$ . Then, for  $h > 0$  sufficiently small,  $\|u\|_{2,h,m} \approx \|\hat{u}\|_{2,h,l}$ , where  
189  $\|\cdot\|_{2,h,m}$  is (3.5) defined on  $\Gamma^m$ .

190 Next, for any  $\boldsymbol{\varphi} \in H^1(\Gamma; \mathbf{S})$ , define

$$(3.6) \quad \|\boldsymbol{\varphi}\|_{0,h}^2 := \|\boldsymbol{\varphi}\|_{L^2(\Gamma)}^2 + h \|\mathbf{n}^T \boldsymbol{\varphi} \mathbf{n}\|_{L^2(\mathcal{E}_{0,h})}^2 + h \|\mathbf{n}^T \boldsymbol{\varphi} \mathbf{n}\|_{L^2(\Sigma_c)}^2,$$

192 and define  $H_h^0$  to be the completion:  $H_h^0(\Gamma; \mathbf{S}) := \overline{H^1(\Gamma; \mathbf{S})}^{\|\cdot\|_{0,h}}$ . By the definition of  
193 the norm,  $H_h^0(\Gamma; \mathbf{S}) \equiv L^2(\Gamma; \mathbf{S}) \oplus L^2(\mathcal{E}_h; \mathbb{R})$ .

194 **3.3. Mixed Skeleton Formulation.** We introduce the following skeleton sub-  
195 spaces

$$(3.7) \quad \mathcal{W}_h(\Gamma) := H_h^2(\Gamma) \cap \mathring{H}^1(\Gamma), \quad \mathcal{V}_h(\Gamma) := \{\boldsymbol{\varphi} \in H_h^0(\Gamma; \mathbf{S}) \mid \boldsymbol{\varphi}^{\text{nn}} = 0 \text{ on } \Sigma_s\},$$

197 when  $\Sigma \neq \emptyset$ , and  $\mathcal{W}_h(\Gamma) := H_h^2(\Gamma)$ ,  $\mathcal{V}_h(\Gamma) := H_h^0(\Gamma; \mathbf{S})$  when  $\Sigma = \emptyset$ ;  $\mathcal{W}_h$  and  $\mathcal{V}_h$  are  
198 mesh-dependent versions of  $\mathcal{W}$  and  $\mathcal{V}$ , respectively.

199 The non-conforming version of (2.5) is as follows, which is based on [39, eqn  
200 (3.10)]. For all  $\varphi \in H_h^0(\Gamma; \mathbf{S})$  and  $v \in H_h^2(\Gamma)$ , define

$$201 \quad (3.8) \quad b_h(\varphi, v) := - \sum_{T \in \mathcal{T}_h} (\varphi, \text{hess}_\Gamma v)_T + \sum_{E \in \mathcal{E}_h} \langle \varphi^{\text{nn}}, [\mathbf{n} \cdot \nabla_\Gamma v] \rangle_E,$$

202 which satisfies the continuity estimate:  $b_h(\varphi, v) \leq \|\varphi\|_{0,h} \|v\|_{2,h}$  for all  $\varphi \in \mathcal{V}_h$  and  
203  $v \in \mathcal{W}_h$ , and define

$$204 \quad (3.9) \quad a(\boldsymbol{\tau}, \boldsymbol{\varphi}) := (\boldsymbol{\tau}, \boldsymbol{\varphi})_\Gamma, \quad \forall \boldsymbol{\tau}, \boldsymbol{\varphi} \in H_h^0(\Gamma; \mathbf{S}).$$

205 Then, if  $w \in \mathcal{W} \subset \mathcal{W}_h(\Gamma)$  and we set  $\boldsymbol{\sigma} := \nabla_\Gamma \nabla_\Gamma w$ , then  $\boldsymbol{\sigma}$  and  $w$  satisfy:

$$206 \quad (3.10) \quad a(\boldsymbol{\sigma}, \boldsymbol{\varphi}) + b_h(\boldsymbol{\varphi}, w) = 0, \quad \forall \boldsymbol{\varphi} \in \mathcal{V}_h.$$

207 Note that the jump terms in (3.8) vanish because  $w \in \mathcal{W}$  and  $\mathbf{n} \cdot \nabla_\Gamma w = 0$  on  $\Sigma_c$ .  
208 Indeed, restricting  $\boldsymbol{\varphi} = \boldsymbol{\sigma}$ , then we have

$$209 \quad (3.11) \quad \|\boldsymbol{\sigma}\|_{L^2(\Gamma)}^2 = a(\boldsymbol{\sigma}, \boldsymbol{\sigma}) = -b_h(\boldsymbol{\sigma}, w) \leq \|\boldsymbol{\sigma}\|_{L^2(\Gamma)} \|\nabla_\Gamma \nabla_\Gamma w\|_{L^2(\Gamma)},$$

210 so  $\boldsymbol{\sigma}$  is the stable  $L^2(\Gamma)$  projection of  $\nabla_\Gamma \nabla_\Gamma w$ .

211 *Remark 3.2.* We also have  $\mathcal{W}_h(\Gamma^m) := H_h^2(\Gamma^m) \cap \dot{H}^1(\Gamma^m)$  and  $\mathcal{V}_h(\Gamma^m) := \{\boldsymbol{\varphi} \in$   
212  $H_h^0(\Gamma^m; \mathbf{S}) \mid \varphi^{\text{nn}} = 0 \text{ on } \Sigma_s^m\}$  defined on the curved triangulation  $\Gamma^m$ , with associated  
213 forms  $b_h^m(\boldsymbol{\varphi}, v)$ ,  $a^m(\boldsymbol{\tau}, \boldsymbol{\varphi})$  defined on  $\Gamma^m$  in the obvious way. These will be used  
214 in our fully discrete version of (3.10) (see (4.7)) which will enable our method for  
215 approximating the surface Hessian of a discrete function.

216 **3.4. Inhomogeneous Boundary Conditions.** We extend the above formu-  
217 lation (3.10) to handle non-vanishing boundary conditions, which is necessary for  
218 approximating the shape operator on surfaces with boundary. First, assume that  
219  $w \in H^3(\Gamma)$  and there exists a function  $g \in H^3(\Gamma)$ , such that  $w = g$  on  $\Sigma$  and  
220  $\partial_n w = \partial_n g$  on  $\Sigma_c$ . Next, construct a function  $\boldsymbol{\rho} \in H^1(\Gamma; \mathbf{S})$ , such that the conormal-  
221 conormal moment satisfies  $\boldsymbol{\sigma}^{\text{nn}} := \mathbf{n}^T \boldsymbol{\sigma} \mathbf{n} = \mathbf{n}^T \boldsymbol{\rho} \mathbf{n}$  on  $\Sigma_s$ . Since the second term in  
222 (3.8) contains boundary integral portions on  $\Sigma_c$ , where  $\mathbf{n} \cdot \nabla_\Gamma w \neq 0$ , then  $\boldsymbol{\sigma}$  and  $w$   
223 satisfy a modified form of (3.10):

$$224 \quad (3.12) \quad a(\boldsymbol{\sigma}, \boldsymbol{\varphi}) + b_h(\boldsymbol{\varphi}, w) = (\varphi^{\text{nn}}, \mathbf{n} \cdot \nabla_\Gamma g)_{\Sigma_c}, \quad \forall \boldsymbol{\varphi} \in \mathcal{V}_h.$$

225 Moreover, writing  $\boldsymbol{\sigma} = \mathring{\boldsymbol{\sigma}} + \boldsymbol{\rho}$ , with  $\mathring{\boldsymbol{\sigma}} \in \mathcal{V}_h$ , we have

$$226 \quad (3.13) \quad a(\mathring{\boldsymbol{\sigma}}, \boldsymbol{\varphi}) = -a(\boldsymbol{\rho}, \boldsymbol{\varphi}) - \mathring{b}_h(\boldsymbol{\varphi}, w), \quad \forall \boldsymbol{\varphi} \in \mathcal{V}_h.$$

227 where we defined  $\mathring{b}_h(\boldsymbol{\varphi}, v) := b_h(\boldsymbol{\varphi}, v) - (\varphi^{\text{nn}}, \mathbf{n} \cdot \nabla_\Gamma v)_{\Sigma_c}$  (i.e. it has no boundary  
228 term). Clearly,  $\|\mathring{\boldsymbol{\sigma}}\|_{L^2(\Gamma)} \leq \|\boldsymbol{\rho}\|_{L^2(\Gamma)} + \|\nabla_\Gamma \nabla_\Gamma w\|_{L^2(\Gamma)}$ . See subsection 4.4 for the  
229 fully discrete method.

230 **3.5. Mapping Properties.** In order to analyze the error in our approximation  
231 scheme (4.9), we need a few results on how functions transform between discrete  
232 surfaces  $\Gamma^m$  and  $\Gamma^l$ , for  $m \neq l$ , as well as how the forms  $b_h^m(\cdot, \cdot)$ ,  $a^m(\cdot, \cdot)$  and  $b_h^l(\cdot, \cdot)$ ,  
233  $a^l(\cdot, \cdot)$  are related.

234 **3.5.1. The Piola Transform.** The tangent space on  $\Gamma^m$  is element-wise defined  
 235 through the mesh  $\mathcal{T}_h^m$ . We require a transformation rule that relates functions in  
 236  $H_h^0(\Gamma^m; \mathbf{S}^m)$  to  $H_h^0(\Gamma^l; \mathbf{S}^l)$  (with  $m \neq l$ ), such that *conormal-conormal continuity*  
 237 is preserved; this is crucial to ensure that the HHJ finite element space in (4.3) is  
 238 continuous. We first recall the surface matrix Piola transform transform from [39,  
 239 Defn. 4.6].

240 **DEFINITION 3.3.** *Recall the curved element mapping discussion in subsection 3.1.*  
 241 *Let  $\mathbf{J} = (\nabla_{T^1} \mathbf{F}_T^m) \bar{\mathbf{P}}_\star \in \mathbb{R}^{3 \times 2}$  where  $\nabla_{T^1}$  is the surface gradient on  $T^1 \in \mathcal{T}_h^1$ ,*  
 242  *$(\nabla_{T^1} \mathbf{F}_T^m) \in \mathbb{R}^{3 \times 3}$ , and  $\bar{\mathbf{P}}_\star \in \mathbb{R}^{3 \times 2}$  is the projection and restriction onto the tan-*  
 243 *gent space of  $T^1$ . Given an extrinsic tensor  $\bar{\varphi} : \Gamma^1 \rightarrow \mathbf{S}^1$  on the piecewise linear*  
 244 *surface  $\Gamma^1$ , we map it (element-wise) to a tensor  $\tilde{\varphi} : \Gamma^m \rightarrow \mathbf{S}^m$ , for any  $m$ , using the*  
 245 *map  $\tilde{\mathbf{x}} = \mathbf{F}_T^m(\bar{\mathbf{x}})$  and*

$$246 \quad (3.14) \quad \tilde{\varphi}(\tilde{\mathbf{x}}) = \text{Piola}(\bar{\varphi})(\tilde{\mathbf{x}}) := \det(\mathbf{Q})^{-1} \mathbf{J} \bar{\mathbf{P}}_\star^T \bar{\varphi}(\bar{\mathbf{x}}) \bar{\mathbf{P}}_\star \mathbf{J}^T,$$

247 where  $\mathbf{Q} = \mathbf{J}^T \mathbf{J}$ . The inverse Piola transform is given by

$$248 \quad (3.15) \quad \bar{\varphi}(\bar{\mathbf{x}}) = \text{Piola}^{-1}(\tilde{\varphi})(\bar{\mathbf{x}}) := \det(\mathbf{Q}) \bar{\mathbf{P}}_\star \mathbf{Q}^{-1} \mathbf{J}^T \tilde{\varphi}(\tilde{\mathbf{x}}) \mathbf{J} \mathbf{Q}^{-1} \bar{\mathbf{P}}_\star^T.$$

249 **Remark 3.4.** A tangential tensor  $\hat{\varphi}$  defined on  $\Gamma^l$  is mapped to a tensor  $\tilde{\varphi}$  on  $\Gamma^m$ ,  
 250 for  $m \neq l$ , through the map  $\Phi^{lm}$  (see (3.1)). In other words,  $\hat{\varphi}$  is mapped to  $\bar{\varphi}$  on  $\Gamma^1$   
 251 using (3.15), and then  $\bar{\varphi}$  is mapped to  $\tilde{\varphi}$  on  $\Gamma^m$  using (3.14).

252 Adopting the hypothesis of Definition 3.3, we recall [39, Prop. 4.7], which states

$$253 \quad (3.16) \quad \tilde{\varphi}^{\text{nn}} \circ \mathbf{F}_T^m = \tilde{\varphi}^{\text{nn}} |(\nabla_{T^1} \mathbf{F}_T^m) \bar{\mathbf{t}}|^{-2}.$$

254 Since  $\mathbf{F}^m$  is piecewise smooth and continuous with respect to the mesh  $\mathcal{T}_h^1$ , it follows  
 255 that  $(\nabla_{T^1} \mathbf{F}_T^m) \bar{\mathbf{t}}$  is single-valued at interelement edges, so  $\tilde{\varphi}$  is conormal-conormal  
 256 continuous if and only if  $\bar{\varphi}$  is. This leads to the following norm equivalence (see [39,  
 257 eqn. (4.15)]):

$$258 \quad (3.17) \quad \|\tilde{\varphi}\|_{0,h,m} \approx \|\bar{\varphi}\|_{0,h,l}, \quad \forall \tilde{\varphi} \in H_h^0(\Gamma^m; \mathbf{S}^m), \quad \text{for all } 1 \leq l, m \leq k, \infty.$$

259 **3.5.2. Mapping Forms.** The following result, which is an improved version of  
 260 [39, Thm. 4.8], is essential for analyzing the geometric error between the approximate  
 261 solution on an approximate domain and exact solution on the exact domain.

262 **THEOREM 3.5.** *Let  $1 \leq l \leq k$  such that  $l < m$ , for  $1 < m \leq k$ , or  $m = \infty$ , and*  
 263 *recall the mapping discussion in subsection 3.1. Let  $\tilde{\sigma} \in H_h^0(\Gamma^m; \mathbf{S}^m)$ ,  $\hat{\sigma} \in H_h^0(\Gamma^l; \mathbf{S}^l)$ ,*  
 264 *and  $\bar{\sigma} \in H_h^0(\Gamma^1; \mathbf{S}^1)$  and assume they are related through the Piola transform (Def-*  
 265 *inition 3.3) in the sense of Remark 3.4. Make the same assumption for  $\tilde{\varphi}$ ,  $\hat{\varphi}$ ,  $\bar{\varphi}$ .*  
 266 *In addition, let  $\tilde{v} \in H_h^2(\Gamma^m)$ ,  $\hat{v} \in H_h^2(\Gamma^l)$ ,  $\bar{v} \in H_h^2(\Gamma^1)$ , where  $\tilde{v}|_T \circ \Phi_T^{1m} = \bar{v}$  and*  
 267  *$\hat{v}|_T \circ \Phi_T^{1l} = \bar{v}$ . Then, there holds*

$$268 \quad (3.18) \quad a^m(\tilde{\sigma}, \tilde{\varphi}) = a^l(\hat{\sigma}, \hat{\varphi}) + O(h^l) \|\hat{\sigma}\|_{L^2(\Gamma^l)} \|\hat{\varphi}\|_{L^2(\Gamma^l)},$$

$$269 \quad b_h^m(\tilde{\varphi}, \tilde{v}) = b_h^l(\hat{\varphi}, \hat{v}) + O(h^l) \|\hat{\varphi}\|_{0,h,l} (\|\hat{v}\|_{2,h,l} + |\hat{v}|_{H^1(\Gamma^l)}) \\
 270 \quad (3.19) \quad - b_h^l(\hat{\varphi}, (\mathbf{F}^m - \mathbf{F}^l) \cdot \text{P}_0 \nabla_{\Gamma^1} \bar{v}) \\
 + \sum_{E^1 \in \mathcal{E}_{\hat{\sigma}, h}^1} \left\langle \tilde{\varphi}^{\text{nn}}, \partial_{\bar{\mathbf{s}}} (\mathbf{F}_T^m - \mathbf{F}_T^l) \cdot \text{P}_0(\boldsymbol{\nu} \times \bar{\mathbf{t}}) \left( \bar{\mathbf{t}} \cdot \nabla_{T^1} \mathcal{I}_h^{1,1} \bar{v} \right) \right\rangle_{E^1},$$

271 where  $\mathcal{I}_h^{1,1}$  is the Lagrange interpolation operator onto piecewise linears on  $\Gamma^1$ ,  $P_0 : L^2(\Gamma^1) \rightarrow L^2(\Gamma^1)$  is the projection onto piecewise constants, and  $\boldsymbol{\nu} \equiv \boldsymbol{\nu} \circ \mathbf{F}_T$  is the unit normal vector of  $T$  (see Theorem 3.1).

274 *Proof.* We start with the result of [39, Thm. 4.8], which already proves (3.18).  
275 Furthermore, we have the following from [39, eqn. (4.17)]:

$$276 \quad (3.20) \quad \begin{aligned} b_h^m(\tilde{\varphi}, \tilde{v}) &= b_h^l(\hat{\varphi}, \hat{v}) + O(h^l) \|\hat{\varphi}\|_{0,h,l} (\|\hat{v}\|_{2,h,l} + |\hat{v}|_{H^1(\Gamma^1)}) \\ &\quad - b_h^l(\tilde{\varphi}, (\mathbf{F}^m - \mathbf{F}^l) \cdot P_0 \nabla_{\Gamma^1} \tilde{v}) + \sum_{E^1 \in \mathcal{E}_{\partial,h}^1} \left\langle \tilde{\varphi}^{\text{nn}}, \beta \tilde{\mathbf{t}} \cdot \nabla_{T^1} \mathcal{I}_h^{1,1} \tilde{v} \right\rangle_{E^1}, \end{aligned}$$

277 where  $\beta = [(\tilde{\mathbf{t}} - \hat{\mathbf{t}}) \times \boldsymbol{\nu}] \cdot \tilde{\mathbf{t}} = (\tilde{\mathbf{t}} - \hat{\mathbf{t}}) \cdot (\boldsymbol{\nu} \times \tilde{\mathbf{t}})$ . Note that the tangent vectors are obtained  
278 from the local element map:

$$279 \quad (3.21) \quad \tilde{\mathbf{t}} = \frac{(\nabla_{T^1} \mathbf{F}_T^m) \bar{\mathbf{t}}}{|(\nabla_{T^1} \mathbf{F}_T^m) \bar{\mathbf{t}}|}, \quad \hat{\mathbf{t}} = \frac{(\nabla_{T^1} \mathbf{F}_T^l) \bar{\mathbf{t}}}{|(\nabla_{T^1} \mathbf{F}_T^l) \bar{\mathbf{t}}|},$$

280 where  $\bar{\mathbf{t}}$  is the tangent vector of the straight element  $E^1 \in \mathcal{E}_{\partial,h}^1$ . Since  $\tilde{\mathbf{t}} \cdot (\boldsymbol{\nu} \times \tilde{\mathbf{t}}) = 0$ ,  
281 we derive another expression for  $\beta$ :

$$282 \quad (3.22) \quad \begin{aligned} \beta &= \left( \frac{|(\nabla_{T^1} \mathbf{F}_T^m) \bar{\mathbf{t}}| \tilde{\mathbf{t}} - |(\nabla_{T^1} \mathbf{F}_T^l) \bar{\mathbf{t}}| \hat{\mathbf{t}}}{|(\nabla_{T^1} \mathbf{F}_T^m) \bar{\mathbf{t}}|} \right) \cdot (\boldsymbol{\nu} \times \tilde{\mathbf{t}}) \\ &= |(\nabla_{T^1} \mathbf{F}_T^l) \bar{\mathbf{t}}|^{-1} ((\nabla_{T^1} \mathbf{F}_T^m) \bar{\mathbf{t}} - (\nabla_{T^1} \mathbf{F}_T^l) \bar{\mathbf{t}}) \cdot (\boldsymbol{\nu} \times \tilde{\mathbf{t}}) \\ &= ((\nabla_{T^1} \mathbf{F}_T^m) \bar{\mathbf{t}} - (\nabla_{T^1} \mathbf{F}_T^l) \bar{\mathbf{t}}) \cdot P_0(\boldsymbol{\nu} \times \tilde{\mathbf{t}}) + O(h^{l+1}), \end{aligned}$$

283 where  $P_0(\boldsymbol{\nu} \times \tilde{\mathbf{t}})$  is the projection onto a piecewise constant vector, and we used (3.2),  
284 (3.3). Moreover, note that  $(\nabla_{T^1} \mathbf{F}_T^m) \bar{\mathbf{t}} - (\nabla_{T^1} \mathbf{F}_T^l) \bar{\mathbf{t}} = \partial_{\bar{s}}(\mathbf{F}_T^m - \mathbf{F}_T^l)$ , where  $\partial_{\bar{s}}$  is the  
285 derivative with respect to arc-length on  $E^1$ . Thus, we get

$$286 \quad (3.23) \quad \begin{aligned} &\sum_{E^1 \in \mathcal{E}_{\partial,h}^1} \left\langle \tilde{\varphi}^{\text{nn}}, \beta \tilde{\mathbf{t}} \cdot \nabla_{T^1} \mathcal{I}_h^{1,1} \tilde{v} \right\rangle_{E^1} \\ &\leq \sum_{E^1 \in \mathcal{E}_{\partial,h}^1} \left\langle \tilde{\varphi}^{\text{nn}}, \partial_{\bar{s}}(\mathbf{F}_T^m - \mathbf{F}_T^l) \cdot \mathbf{C}_{E^1} \right\rangle_{E^1} + O(h^l) \|\hat{\varphi}\|_{0,h,l} |\hat{v}|_{H^1(\Gamma^1)}, \end{aligned}$$

287 where  $\mathbf{C}_{E^1} := P_0(\boldsymbol{\nu} \times \tilde{\mathbf{t}}) \left( \tilde{\mathbf{t}} \cdot \nabla_{T^1} \mathcal{I}_h^{1,1} \tilde{v} \right)$  is defined on  $E^1 \in \mathcal{E}_{\partial,h}^1$ , and we used equivalence  
288 of norms. The result (3.19) then follows.  $\square$

289 A simple consequence of Theorem 3.5 is

$$290 \quad (3.24) \quad b_h^m(\varphi, v) = b_h^l(\hat{\varphi}, \hat{v}) + O(h^{l-1}) \|\hat{\varphi}\|_{0,h,l} \|\hat{v}\|_{2,h,l}.$$

## 291 4. Finite Element Approximation.

292 **4.1. Curved Lagrange Spaces.** Let  $r \geq 0$  be an integer and  $m \geq 1$  be an  
293 integer or  $\infty$ . The (continuous) Lagrange finite element space of degree  $r+1$  is  
294 defined on  $\Gamma^m$  via the mapping  $\mathbf{F}_T^m$ :

$$295 \quad (4.1) \quad W_h^{m,r+1} \equiv W_h^{m,r+1}(\Gamma^m) := \{v \in H_h^2(\Gamma^m) \mid v|_T \circ \mathbf{F}_T^m \in \mathcal{P}_{r+1}(T^1), \forall T \in \mathcal{T}_h^m\},$$

296 where we will usually suppress the  $r+1$  superscript, i.e. we make the abbreviation  
297  $W_h^{m,r+1} \equiv W_h^m$ . For the case  $m = \infty$  (the exact domain) we simply write  $W_h$ .



298 Again, owing to the continuous embedding  $H_h^2(\Gamma^1) \hookrightarrow C^0(\overline{\Gamma^1})$  (see [40, Thm.  
299 4.2]), we can define the Lagrange interpolation operator  $\mathcal{I}_h^1 : H_h^2(\Gamma^1) \rightarrow W_h^1$ , [5]  
300 defined on each element  $T^1 \in \mathcal{T}_h^1$  by

$$301 \quad (4.2) \quad (\mathcal{I}_h^1 v)(\mathbf{x}) - v(\mathbf{x}) = 0, \quad \int_{E^1} (\mathcal{I}_h^1 v - v)q \, ds = 0, \quad \int_{T^1} (\mathcal{I}_h^1 v - v)\eta \, dS = 0,$$

302 for all vertices  $\mathbf{x}$  of  $T^1$ , all  $q \in \mathcal{P}_{r-1}(E^1)$  (and all  $E^1 \in \partial T^1$ ), and all  $\eta \in \mathcal{P}_{r-2}(T^1)$ .  
303 Then, given  $v \in H_h^2(\Gamma^m)$ , we define the global interpolation operator,  $\mathcal{I}_h^m : H_h^2(\Gamma^m) \rightarrow$   
304  $W_h^m$ , element-wise through  $\mathcal{I}_h^m v|_{T^m} \circ \mathbf{F}_{T^m}^m := \mathcal{I}_h^1(v \circ \mathbf{F}_{T^m}^m)$ . The approximation proper-  
305 ties of  $\mathcal{I}_h^m$  are standard. We also denote  $\mathcal{I}_h^{m,s}$  to be the above Lagrange interpolant  
306 on  $\Gamma^m$  onto continuous piecewise polynomials of degree  $s$ , and we make the following  
307 abbreviation  $\mathcal{I}_h^{m,r+1} \equiv \mathcal{I}_h^m$ .

308 **4.2. The HHJ Finite Element Space.** We give a brief overview of the surface  
309 HHJ space; see [39, Sec. 5.2] for more details. On the piecewise linear surface trian-  
310 gulation  $\Gamma^1$ , we start with a space of tangential, tensor-valued functions with special  
311 continuity properties. Let

$$312 \quad \mathcal{M}_{\text{nn}}^1(\Gamma^1) := \{\varphi \in L^2(\Gamma^1; \mathbf{S}^1) \mid \varphi|_{T^1} \in H^1(T^1; \mathbf{S}^1) \, \forall T^1 \in \mathcal{T}_h^1, \text{ with } \varphi \text{ cn-cn contin.}\},$$

313 where ‘‘cn-cn contin.’’ means the *conormal-conormal continuity* condition that holds  
314 at inter-element boundaries, i.e. for any pair of triangles  $(T_a^1, T_b^1)$  in  $\mathcal{T}_h^1$  that share  
315 an edge  $E^1 = \overline{T_a^1} \cap \overline{T_b^1}$ , we have  $\mathbf{n}_a^T \varphi \mathbf{n}_a|_{E^1} = \mathbf{n}_b^T \varphi \mathbf{n}_b|_{E^1}$ , where  $\mathbf{n}_a$  ( $\mathbf{n}_b$ ) is the  
316 outer conormal of  $\partial T_a^1$  ( $\partial T_b^1$ ); note that, in general,  $\mathbf{n}_a \neq -\mathbf{n}_b$  (on  $E^1$ ). Clearly,  
317  $\mathcal{M}_{\text{nn}}^1(\Gamma^1) \subset H_h^0(\Gamma^1; \mathbf{S}^1)$ . For  $1 \leq m \leq k, \infty$ , where  $\Gamma^\infty \equiv \Gamma$ , we also have the space

$$318 \quad \mathcal{M}_{\text{nn}}^m(\Gamma^m) := \{\varphi \in L^2(\Gamma^m; \mathbf{S}^m) \mid \varphi \circ \mathbf{F}^m := \text{Piola}(\bar{\varphi}), \bar{\varphi} \in \mathcal{M}_{\text{nn}}^1(\Gamma^1)\},$$

319 where the Piola transform is defined elementwise, using  $\mathbf{F}^m$ ; by (3.16),  $\mathcal{M}_{\text{nn}}^m(\Gamma^m)$  also  
320 satisfies the conormal-conormal continuity property.

321 The conforming, HHJ finite element space on  $\Gamma^1$ , of degree  $r \geq 0$ , is defined by  
322  $V_h^1 := \{\varphi \in \mathcal{M}_{\text{nn}}^1(\Gamma^1) \mid \varphi|_{T^1} \in \mathcal{P}_r(T^1; \mathbf{S}^1), \, \forall T^1 \in \mathcal{T}_h^1\}$ . Using the Piola transform,  
323 for  $1 \leq m \leq k, \infty$ , we also have

$$324 \quad (4.3) \quad V_h^m := \{\varphi \in \mathcal{M}_{\text{nn}}^m(\Gamma^m) \mid \varphi \circ \mathbf{F}^m := \text{Piola}(\bar{\varphi}), \bar{\varphi} \in V_h^1\}.$$

325 We note the following norm equivalence in [39, eqn. (5.5)]:

$$326 \quad (4.4) \quad \|\varphi\|_{0,h,m} \approx \|\varphi\|_{L^2(\Gamma^m)}, \, \forall \varphi \in V_h^m.$$

327 There exists an interpolation operator  $\Pi_h^m : \mathcal{M}_{\text{nn}}^m(\Gamma^m) \rightarrow V_h^m$ , defined element-  
328 wise, that satisfies many basic approximation results which can be found in [3, Supp.  
329 Mater.], [39, sec. 5.2]. For simplicity, we describe the operator on  $\Gamma^1$  only, i.e.  
330  $\Pi_h^1 : \mathcal{M}_{\text{nn}}^1(\Gamma^1) \rightarrow V_h^1$ , [10, 5] is defined on each element  $T^1 \in \mathcal{T}_h^1$  by

$$331 \quad (4.5) \quad \int_{E^1} \mathbf{n}^T [\Pi_h^1 \varphi - \varphi] \mathbf{n} \, q \, ds = 0, \quad \int_{T^1} [\Pi_h^1 \varphi - \varphi] : \boldsymbol{\eta} \, dS = 0,$$

332 for all  $q \in \mathcal{P}_r(E^1)$  (and all  $E^1 \in \partial T^1$ ), and all  $\boldsymbol{\eta} \in \mathcal{P}_{r-1}(T^1; \mathbf{S})$ . We note that the  
333 Degrees-of-Freedom (DoFs) for  $V_h^1$  are given by (4.5), [10, Lem. 3], [27]. On affine

334 elements, we have a Fortin like property involving  $b_h^1(\cdot, \cdot)$ , [10, 5, 8]:

$$\begin{aligned}
& b_h^1(\boldsymbol{\varphi} - \Pi_h^1 \boldsymbol{\varphi}, \theta_h v_h) = 0, \quad \forall \boldsymbol{\varphi} \in H_h^0(\Gamma^1; \mathbf{S}^1), \quad v_h \in W_h^1, \\
335 \quad (4.6) \quad & b_h^1(\boldsymbol{\varphi}_h, (v - \mathcal{I}_h^1 v) \theta_h) = 0, \quad \forall \boldsymbol{\varphi}_h \in V_h^1, \quad v \in H_h^2(\Gamma^1), \\
& (\boldsymbol{\varphi}_h^{\text{nn}}, \partial_{\bar{s}}(v - \mathcal{I}_h^1 v) \eta_h)_{\mathcal{E}_{\partial, h}^1} = 0, \quad \forall \boldsymbol{\varphi}_h \in V_h^1, \quad v \in H_h^2(\Gamma^1),
\end{aligned}$$

336 which holds for *any* piecewise constant functions  $\theta_h$  ( $\eta_h$ ) defined on  $\mathcal{T}_h^1$  ( $\mathcal{E}_{\partial, h}^1$ ); the  
337 first two properties are noted in [10, 5, 8].

338 **4.3. The HHJ Projection.** We pose (3.10) on  $\Gamma^m$  with continuous skeleton  
339 spaces denoted  $\mathcal{V}_h^m \equiv \mathcal{V}_h(\Gamma^m)$  and  $\mathcal{W}_h^m \equiv \mathcal{W}_h(\Gamma^m)$ . Fixing the polynomial degree  
340  $r \geq 0$ , the conforming finite element spaces are  $V_h^m \subset \mathcal{V}_h^m$ ,  $W_h^m \subset \mathcal{W}_h^m$ , where  
341 we abuse notation by now *enforcing essential boundary conditions* directly in the  
342 definitions of  $V_h^m$  and  $W_h^m$ . The finite element approximation to (3.10) is as follows.  
343 Given any  $\hat{w}_h \in \mathcal{W}_h^m$ , find  $\hat{\boldsymbol{\sigma}}_h \in V_h^m$ , such that

$$344 \quad (4.7) \quad a^m(\hat{\boldsymbol{\sigma}}_h, \hat{\boldsymbol{\varphi}}_h) + b_h^m(\hat{\boldsymbol{\varphi}}_h, \hat{w}_h) = 0, \quad \forall \hat{\boldsymbol{\varphi}}_h \in V_h^m.$$

345 Since  $a^m(\cdot, \cdot)$  is continuous and coercive over  $V_h^m$ , by (4.4), we get

$$\begin{aligned}
346 \quad (4.8) \quad & \|\hat{\boldsymbol{\sigma}}_h\|_{L^2(\Gamma^m)}^2 = a^m(\hat{\boldsymbol{\sigma}}_h, \hat{\boldsymbol{\sigma}}_h) = -b_h^m(\hat{\boldsymbol{\sigma}}_h, w_h) \leq \|\hat{\boldsymbol{\sigma}}_h\|_{0, h, m} \|\hat{w}_h\|_{2, h, m} \\
& \leq C \|\hat{\boldsymbol{\sigma}}_h\|_{L^2(\Gamma^m)} \|\hat{w}_h\|_{2, h, m},
\end{aligned}$$

347 for some independent constant  $C > 0$ . Thus,  $\hat{\boldsymbol{\sigma}}_h$  is a stable  $L^2(\Gamma^m)$  projection. In a  
348 sense,  $\hat{\boldsymbol{\sigma}}_h$  can be viewed as a discrete Hessian of  $\hat{w}_h$  (see the error estimate in (4.22)).

349 **4.4. Inhomogeneous Boundary Conditions.** We modify (4.7) to incorporate  
350 non-zero boundary conditions, i.e. we give a discrete version of (3.12). For any  
351  $w \in H^{r+3}(\Gamma)$ , we define  $\tilde{w} := w \circ \boldsymbol{\Psi}^m \in H_h^2(\Gamma^m)$ , and set  $\tilde{\boldsymbol{\xi}} := (\nabla_{\Gamma} w) \circ \boldsymbol{\Psi}^m$ . Then,  
352 we seek  $\hat{\boldsymbol{\sigma}}_h = \hat{\boldsymbol{\sigma}}_h^{\circ} + \hat{\boldsymbol{\rho}}_h$ , with  $\hat{\boldsymbol{\sigma}}_h^{\circ} \in V_h^m$ , such that

$$353 \quad (4.9) \quad a^m(\hat{\boldsymbol{\sigma}}_h^{\circ}, \hat{\boldsymbol{\varphi}}_h) = -a^m(\hat{\boldsymbol{\rho}}_h, \hat{\boldsymbol{\varphi}}_h) - b_h^m(\hat{\boldsymbol{\varphi}}_h, \tilde{w}) + \left( \hat{\boldsymbol{\varphi}}_h^{\text{nn}}, \hat{\mathbf{n}} \cdot \tilde{\boldsymbol{\xi}} \right)_{\Sigma_c^m}, \quad \forall \hat{\boldsymbol{\varphi}}_h \in V_h^m,$$

354 where  $\hat{\boldsymbol{\rho}}_h := B_h^m \tilde{\boldsymbol{\rho}}$ , with  $\tilde{\boldsymbol{\rho}}$  satisfying  $\boldsymbol{\rho} \circ \boldsymbol{\Psi}^m = \tilde{\boldsymbol{\rho}}$ , and  $B_h^m : H_h^0(\Gamma^m) \rightarrow V_h^m$  is the  
355 projection on  $\Gamma^m$ , i.e.

$$356 \quad (4.10) \quad (\hat{\boldsymbol{\rho}}_h - \tilde{\boldsymbol{\rho}}, \hat{\boldsymbol{\varphi}}_h)_{\mathcal{T}_h^m} + (\hat{\mathbf{n}}^T [\hat{\boldsymbol{\rho}}_h - \tilde{\boldsymbol{\rho}}] \hat{\mathbf{n}}, \hat{\boldsymbol{\varphi}}_h^{\text{nn}})_{\mathcal{E}_h^m} = 0, \quad \forall \hat{\boldsymbol{\varphi}}_h \in V_h^m,$$

357 which satisfies the approximation property  $\|\hat{\boldsymbol{\rho}}_h - \tilde{\boldsymbol{\rho}}\|_{0, h, m} \leq Ch^{\min(r+1, m)} \|\boldsymbol{\rho}\|_{H^{r+1}(\Gamma)}$ .

358 Choosing  $\hat{\boldsymbol{\varphi}}_h = \hat{\boldsymbol{\sigma}}_h^{\circ}$  in (4.9), we have

$$\begin{aligned}
359 \quad (4.11) \quad & \|\hat{\boldsymbol{\sigma}}_h^{\circ}\|_{L^2(\Gamma^m)}^2 = -a^m(\hat{\boldsymbol{\rho}}_h, \hat{\boldsymbol{\sigma}}_h^{\circ}) - b_h^m(\hat{\boldsymbol{\sigma}}_h^{\circ}, \tilde{w}) - \left( \hat{\mathbf{n}}^T \hat{\boldsymbol{\sigma}}_h^{\circ} \hat{\mathbf{n}}, \hat{\mathbf{n}} \cdot [\nabla_{\Gamma^m} \tilde{w} - \tilde{\boldsymbol{\xi}}] \right)_{\Sigma_c^m} \\
& \leq \|\hat{\boldsymbol{\rho}}_h\|_{L^2(\Gamma^m)} \|\hat{\boldsymbol{\sigma}}_h^{\circ}\|_{L^2(\Gamma^m)} + \|\hat{\boldsymbol{\sigma}}_h^{\circ}\|_{0, h, m} \|\tilde{w}\|_{2, h, m} + C \|\hat{\boldsymbol{\sigma}}_h^{\circ}\|_{L^2(\Gamma^m)} \|w\|_{H^2(\Gamma)},
\end{aligned}$$

360 where, since  $\text{id}_{\Gamma^m}^k = \mathcal{I}_h^m \text{id}_{\Gamma}^k$ , applying straightforward change of variables, standard  
361 interpolation estimates, and an inverse estimate, give (see [39])

$$\begin{aligned}
362 \quad (4.12) \quad & \left| \left( \hat{\mathbf{n}}^T \hat{\boldsymbol{\sigma}}_h^{\circ} \hat{\mathbf{n}}, \hat{\mathbf{n}} \cdot [\nabla_{\Gamma^m} \tilde{w} - \tilde{\boldsymbol{\xi}}] \right)_{\Sigma_c^m} \right| \leq O(h^{1/2}) \|\hat{\boldsymbol{\sigma}}_h^{\circ}\|_{L^2(\Sigma^m)} \|w\|_{H^2(\Gamma)} \\
& \leq C \|\hat{\boldsymbol{\sigma}}_h^{\circ}\|_{L^2(\Gamma^m)} \|w\|_{H^2(\Gamma)}.
\end{aligned}$$

363 By equivalence of norms,  $\|\tilde{w}\|_{2,h,m} \approx \|w\|_{2,h} \equiv \|\nabla_\Gamma \nabla_\Gamma w\|_{L^2(\Gamma)}$  and  $\|\mathring{\sigma}_h\|_{L^2(\Gamma^m)} \approx$   
 364  $\|\mathring{\sigma}_h\|_{0,h,m}$ , we obtain

$$365 \quad (4.13) \quad \|\mathring{\sigma}_h\|_{0,h,m} \leq C (\|\hat{\rho}_h\|_{L^2(\Gamma^m)} + \|w\|_{H^2(\Gamma)}),$$

366 for some constant  $C > 0$  that does not depend on  $h$ . Thus, the projection is stable.

367 **4.5. Error Analysis.** The stability of the surface HHJ method, as well as its  
 368 convergence, depends crucially on the following choice of surface approximation: let  
 369  $\widetilde{\mathbf{F}}_T^m : T^1 \rightarrow T^m$ , for all  $T^1 \in \mathcal{T}_h^1$  and  $1 \leq m \leq k$ , be given by

$$370 \quad (4.14) \quad \mathbf{F}_T^m \equiv \widetilde{\mathbf{F}}_T^m := \mathcal{I}_h^{1,m} \mathbf{F}_T \equiv \mathcal{I}_h^{1,m} \Psi_T^1,$$

371 where  $\mathcal{I}_h^{1,m}$  is the Lagrange interpolation operator in (4.2) onto degree  $m$  polynomials;  
 372 we simplify the notation by writing  $\mathbf{F}_T^m \equiv \widetilde{\mathbf{F}}_T^m$ . This choice is necessary to guarantee  
 373 optimal convergence of the HHJ method when  $m = r + 1$ . If  $m > r + 1$ , the standard  
 374 Lagrange interpolant can be used.

375 For the convergence analysis, we assume  $w \in H^{r+3}(\Gamma)$ , where  $r \geq 0$  is the degree  
 376 of the HHJ space. Let  $\sigma := \nabla_\Gamma \nabla_\Gamma w \in H^{r+1}(\Gamma; \mathbf{S})$ , and note that  $\sigma$  satisfies (3.12),  
 377 where  $\rho \in H^{r+1}(\Gamma; \mathbf{S})$  is such that  $\mathbf{n}^T \sigma \mathbf{n} = \mathbf{n}^T \rho \mathbf{n}$  on  $\Sigma_s$ . Next, we introduce an  
 378 intermediate discrete (finite dimensional) problem posed on the exact surface. Let  $\rho_h$   
 379 be the  $L^2(\Gamma)$  projection of  $\rho$  onto  $V_h$ , i.e.  $\rho_h \in V_h$  satisfies  $a(\rho_h, \varphi_h) = a(\rho, \varphi_h)$  for  
 380 all  $\varphi_h \in V_h$ . Then, we write  $\sigma_h = \mathring{\sigma}_h + \rho_h$ , where  $\mathring{\sigma}_h \in V_h$  satisfies

$$381 \quad (4.15) \quad a(\mathring{\sigma}_h, \varphi_h) = -a(\rho, \varphi_h) - b_h(\varphi_h, w) + (\varphi_h^{\text{nn}}, \mathbf{n} \cdot \nabla_\Gamma w)_{\Sigma_c}, \quad \forall \varphi_h \in V_h,$$

382 where  $\mathring{\sigma}_h$  can be viewed as a stable projection. Comparing (4.15) with (3.13), by  
 383 standard finite element analysis, utilizing Galerkin orthogonality and interpolation  
 384 estimates, we have that  $\|\mathring{\sigma} - \mathring{\sigma}_h\|_{L^2(\Gamma)} \leq \|\mathring{\sigma} - \Pi_h \mathring{\sigma}\|_{L^2(\Gamma)} = O(h^{r+1})$ , which implies

$$385 \quad (4.16) \quad \|\sigma - \sigma_h\|_{L^2(\Gamma)} \leq O(h^{r+1}).$$

386 Next, let  $\hat{\sigma}_h$  solve (4.9). To facilitate estimating the error between  $\hat{\sigma}_h$  and the  
 387 exact surface Hessian  $\sigma$ , we map  $\sigma_h$  to the discrete surface  $\Gamma^m$ , i.e. by letting  $\mathring{\hat{\sigma}}_h \in V_h^m$   
 388 satisfy  $\mathring{\hat{\sigma}}_h \circ \Psi^m = \text{Piola}(\mathring{\hat{\sigma}}_h)$  (recall (3.14)), and then compare  $\mathring{\hat{\sigma}}_h$  to  $\mathring{\hat{\sigma}}_h$ .

389 So, we apply the results of Theorem 3.5 to (4.15) to find that  $\mathring{\hat{\sigma}}_h \in V_h^m$  satisfies

$$390 \quad (4.17) \quad \begin{aligned} a^m(\mathring{\hat{\sigma}}_h, \hat{\varphi}_h) &= -a^m(\tilde{\rho}, \hat{\varphi}_h) - b_h^m(\hat{\varphi}_h, \tilde{w}) + \left( \hat{\varphi}_h^{\text{nn}}, \hat{\mathbf{n}} \cdot \hat{\xi} \right)_{\Sigma_c^m} \\ &+ O(h^m) \left( \|\mathring{\hat{\sigma}}_h\|_{L^2(\Gamma^m)} + \|\tilde{\rho}\|_{L^2(\Gamma^m)} \right) \|\hat{\varphi}_h\|_{L^2(\Gamma^m)} \\ &+ O(h^m) \|\hat{\varphi}_h\|_{0,h,m} (\|\tilde{w}\|_{2,h,m} + |\tilde{w}|_{H^1(\Gamma^m)}) \\ &- b_h^1(\hat{\varphi}_h, (\mathbf{F} - \mathbf{F}^m) \cdot \text{P}_0 \nabla_{\Gamma^1} \tilde{w}_h) + (\hat{\varphi}_h^{\text{nn}}, \partial_{\bar{s}}(\mathbf{F}_T - \mathbf{F}_T^m) \cdot \mathbf{C}_{E^1})_{\mathcal{E}_{\partial,h}^1}, \end{aligned}$$

391 for all  $\hat{\varphi}_h$  in  $V_h^m$ , where  $\mathbf{C}_{E^1}$  is a constant vector for each  $E^1 \in \mathcal{E}_{\partial,h}^1$ . We also used  
 392 that

$$393 \quad (4.18) \quad \left| (\varphi_h^{\text{nn}}, \mathbf{n} \cdot \nabla_\Gamma w)_E - \left( \hat{\varphi}_h^{\text{nn}}, \hat{\mathbf{n}} \cdot \hat{\xi} \right)_{E^m} \right| \leq O(h^m) \|\hat{\varphi}_h\|_{0,h,m} (\|\tilde{w}\|_{2,h,m} + |\tilde{w}|_{H^1(\Gamma^m)}),$$

394 for all  $E \in \mathcal{E}_{\partial,h}$  where  $E^m = E \circ \Psi^m$ . Next, we make note of the assumption on  $\mathbf{F}^m$   
 395 (4.14), use (4.6), and take advantage of equivalent norms to obtain

$$396 \quad (4.19) \quad \begin{aligned} a^m(\mathring{\hat{\sigma}}_h, \hat{\varphi}_h) &= -a^m(\tilde{\rho}, \hat{\varphi}_h) - b_h^m(\hat{\varphi}_h, \tilde{w}) + \left( \hat{\varphi}_h^{\text{nn}}, \hat{\mathbf{n}} \cdot \hat{\xi} \right)_{\Sigma_c^m} \\ &+ O(h^m) \|\hat{\varphi}_h\|_{L^2(\Gamma^m)} (\|\rho\|_{L^2(\Gamma)} + \|w\|_{H^2(\Gamma)}), \quad \forall \hat{\varphi}_h \in V_h^m, \end{aligned}$$

397 where we also note that  $C\|\mathring{\boldsymbol{\sigma}}_h\|_{L^2(\Gamma^m)} \leq \|\mathring{\boldsymbol{\sigma}}_h\|_{L^2(\Gamma)} \leq \|\boldsymbol{\rho}\|_{L^2(\Gamma)} + \|\nabla_\Gamma \nabla_\Gamma w\|_{L^2(\Gamma)}$ , for  
 398 some independent constant  $C > 0$ . Comparing (4.19) against (4.9), we get

(4.20)

$$399 \quad a^m \left( \mathring{\boldsymbol{\sigma}}_h - \hat{\boldsymbol{\sigma}}_h, \hat{\boldsymbol{\varphi}}_h \right) = a^m \left( \hat{\boldsymbol{\rho}}_h - \tilde{\boldsymbol{\rho}}, \hat{\boldsymbol{\varphi}}_h \right) + O(h^m) \|\hat{\boldsymbol{\varphi}}_h\|_{L^2(\Gamma^m)} \left( \|\boldsymbol{\rho}\|_{L^2(\Gamma)} + \|w\|_{H^2(\Gamma)} \right) \\
 \leq \|\hat{\boldsymbol{\varphi}}_h\|_{L^2(\Gamma^m)} \left[ O(h^{r+1}) \|\boldsymbol{\rho}\|_{H^{r+1}(\Gamma)} + O(h^m) \left( \|\boldsymbol{\rho}\|_{L^2(\Gamma)} + \|w\|_{H^2(\Gamma)} \right) \right],$$

400 for all  $\hat{\boldsymbol{\varphi}}_h$  in  $V_h^m$ . Therefore, we get  $\|\mathring{\boldsymbol{\sigma}}_h - \hat{\boldsymbol{\sigma}}_h\|_{L^2(\Gamma^m)} \leq Ch^{\min(r+1, m)}$ , where the  
 401 constant  $C$  depends on the  $H^{r+3}(\Gamma)$  norm of  $\Gamma$ . Thus, we obtain

$$402 \quad (4.21) \quad \|\mathring{\boldsymbol{\sigma}}_h - \hat{\boldsymbol{\sigma}}_h\|_{L^2(\Gamma^m)} \leq Ch^{\min(r+1, m)}.$$

403 Combining the above results yields the following theorem.

404 **THEOREM 4.1.** *Assume  $r \geq 0$  is an integer, let  $w \in H^{r+3}(\Gamma)$ , and set  $\boldsymbol{\sigma} :=$   
 405  $\nabla_\Gamma \nabla_\Gamma w \in \mathbf{S}$ . Furthermore, assume  $r \geq 0$  is the degree of  $V_h^m$ , and let  $\hat{\boldsymbol{\sigma}}_h = \mathring{\boldsymbol{\sigma}}_h + \hat{\boldsymbol{\rho}}_h$ ,  
 406 with  $\mathring{\boldsymbol{\sigma}}_h \in V_h^m$  satisfying (4.9) and  $\hat{\boldsymbol{\rho}}_h$  defined through (4.10). If  $m \geq r + 1$ , then*

$$407 \quad (4.22) \quad \|\boldsymbol{\sigma} - \hat{\boldsymbol{\sigma}}_h \circ (\boldsymbol{\Psi}^m)^{-1}\|_{0, h} \leq Ch^{r+1},$$

408 where  $C > 0$  depends on the domain  $\Gamma$  and the shape regularity of the mesh.

409 *Proof.* Let  $\boldsymbol{\sigma}_h$  be the discrete solution (defined on the exact surface) computed  
 410 through (4.15), and let  $\tilde{\boldsymbol{\sigma}}_h \in V_h^m$  satisfy  $\boldsymbol{\sigma}_h \circ \boldsymbol{\Psi}^m = \text{Piola}(\tilde{\boldsymbol{\sigma}}_h)$ . It is straightforward to  
 411 derive the estimate  $\|\boldsymbol{\sigma}_h - \tilde{\boldsymbol{\sigma}}_h \circ (\boldsymbol{\Psi}^m)^{-1}\|_{0, h} \leq O(h^{r+1}) \|\tilde{\boldsymbol{\sigma}}_h\|_{0, h, m}$  (see [39, Thm. 6.4]).  
 412 Then, combining with (4.16) and (4.21) through the triangle inequality, we obtain  
 413 (4.22).  $\square$

414 *Remark 4.2.* The ‘‘exact’’ data  $\tilde{w}$  and  $\tilde{\boldsymbol{\xi}}$  can be replaced by their interpolants,  
 415  $\mathcal{I}_h^m \tilde{w}$  and  $\mathcal{I}_h^m \tilde{\boldsymbol{\xi}}$ , without affecting the stability or accuracy of the scheme in (4.9).

416 In a sense, our scheme is a kind of Hessian recovery of the given discrete data  
 417  $\mathcal{I}_h^m \tilde{w}$ , including boundary data  $\mathcal{I}_h^m \tilde{\boldsymbol{\xi}}$  and  $\hat{\boldsymbol{\rho}}_h$ . We note that another method of Hessian  
 418 recovery for the HJ element, developed for flat domains, is given in [28].

419 **5. Approximating the Shape Operator.** Recall that, for any  $C^2$  surface  $\Gamma$ ,  
 420 we have the identity map  $\text{id}_\Gamma : \Gamma \rightarrow \Gamma$  given by  $\mathbf{x} = \text{id}_\Gamma(\mathbf{x})$  for all  $\mathbf{x} \in \Gamma$ , and  
 421  $\nabla_\Gamma \text{id}_\Gamma = \mathbf{P}$  (tangent space projection). In addition, we have the shape operator  $\nabla_\Gamma \boldsymbol{\nu}$   
 422 that satisfies (SM2.4):  $\nabla_\Gamma \boldsymbol{\nu} = \kappa^1 \mathbf{d}_1 \otimes \mathbf{d}_1 + \kappa^2 \mathbf{d}_2 \otimes \mathbf{d}_2$ , where  $\kappa^1, \kappa^2$  are the *principle*  
 423 *curvatures* of  $\Gamma$ , with  $\kappa^1 \geq \kappa^2$ , and  $\mathbf{d}_1, \mathbf{d}_2$  are the *principle directions* (which are  
 424 tangent to  $\Gamma$ ).

425 **5.1. An Identity.** We exploit the following result in our method.

426 **PROPOSITION 5.1.** *If  $\Gamma$  is  $C^2$ , then at every point of  $\Gamma$ , there holds*

$$427 \quad (5.1) \quad \nabla_\Gamma \nabla_\Gamma \text{id}_\Gamma^k = -\nu^k [\nabla_\Gamma \boldsymbol{\nu}], \quad \text{for } k = 1, 2, 3.$$

428 *Proof.* Let  $\{U, \boldsymbol{\chi}\}$  be a local chart such that the open set  $\Upsilon := \boldsymbol{\chi}(U)$  is contained  
 429 in  $\Gamma$ . Without loss of generality, we derive the identity on  $\Upsilon$  only. Furthermore, since  
 430  $\nabla_\Gamma \nabla_\Gamma, \boldsymbol{\nu}$ , and  $\nabla_\Gamma \boldsymbol{\nu}$ , are independent of the parametrization, we take advantage of a  
 431 particular choice and assume  $\boldsymbol{\chi}$  has the form  $\boldsymbol{\chi} = (\chi^1, \chi^2, \chi^3)$  with

$$432 \quad (5.2) \quad \chi^1(u^1, u^2) = u^1, \quad \chi^2(u^1, u^2) = u^2, \quad \chi^3(u^1, u^2) = h(u^1, u^2),$$

433 where  $h \in C^2$  is a height function. With this, the metric,  $g_{\alpha\beta}$ , and its inverse,  $g^{\alpha\beta}$   
434 are given by

$$435 \quad (5.3) \quad g_{\alpha\beta} = \delta_{\alpha\beta} + (\partial_\alpha h)(\partial_\beta h), \quad g^{\alpha\beta} = \delta^{\alpha\beta} - \frac{(\partial_\alpha h)(\partial_\beta h)}{1 + (\partial_\mu h)^2},$$

436 which then yields the following simplified form of the Christoffel symbols  $\Gamma_{ij}^k$  (of the  
437 second kind) (see (SM1.1)):

$$438 \quad (5.4) \quad \Gamma_{\alpha\beta}^\gamma = \frac{1}{1 + (\partial_\mu h)^2} (\partial_\gamma h)(\partial_\alpha \partial_\beta h), \quad 1 \leq \alpha, \beta, \gamma \leq 2.$$

439 Let  $\mathbf{e}_\alpha = \partial_\alpha \boldsymbol{\chi}$ , for  $\alpha = 1, 2$ . Using (SM2.3), we have that  $\mathbf{e}_\alpha^T \left( \nabla_\Gamma \nabla_\Gamma \text{id}_\Gamma^k \right) \mathbf{e}_\beta =$   
440  $(\partial_\alpha \partial_\beta \chi^k) - \Gamma_{\alpha\beta}^\mu (\partial_\mu \chi^k)$ , so

$$441 \quad (5.5) \quad \mathbf{e}_\alpha^T \left( \nabla_\Gamma \nabla_\Gamma \text{id}_\Gamma^k \right) \mathbf{e}_\beta = \begin{cases} - (1 + (\partial_\mu h)^2)^{-1} (\partial_k h)(\partial_\alpha \partial_\beta h), & \text{if } 1 \leq k \leq 2, \\ (1 + (\partial_\mu h)^2)^{-1} (\partial_\alpha \partial_\beta h), & \text{if } k = 3. \end{cases}$$

442 Next, note that the normal vector is given by

$$443 \quad (5.6) \quad \boldsymbol{\nu} \circ \boldsymbol{\chi} = \frac{(-\partial_1 h, -\partial_2 h, 1)}{(1 + (\partial_\mu h)^2)^{1/2}}.$$

444 In local coordinates,  $[\nabla_\Gamma \boldsymbol{\nu}] \circ \boldsymbol{\chi} = (\partial_\omega \boldsymbol{\nu}) g^{\omega\theta} (\partial_\theta \boldsymbol{\chi})^T$  by (SM2.2), so then

$$445 \quad (5.7) \quad \begin{aligned} \mathbf{e}_\alpha^T [\nabla_\Gamma \boldsymbol{\nu}] \mathbf{e}_\beta &= (\partial_\alpha \boldsymbol{\chi}) \cdot (\partial_\omega \boldsymbol{\nu}) g^{\omega\theta} (\partial_\theta \boldsymbol{\chi}) \cdot (\partial_\beta \boldsymbol{\chi}) = -(\partial_\omega \partial_\alpha \boldsymbol{\chi}) \cdot \boldsymbol{\nu} g^{\omega\theta} g_{\theta\beta} \\ &= -(\partial_\alpha \partial_\beta \boldsymbol{\chi}) \cdot \boldsymbol{\nu} = -(\partial_\alpha \partial_\beta h) \nu^3 = -\frac{\partial_\alpha \partial_\beta h}{(1 + (\partial_\mu h)^2)^{1/2}}, \end{aligned}$$

446 which implies that

$$447 \quad (5.8) \quad \mathbf{e}_\alpha^T (\nu^k [\nabla_\Gamma \boldsymbol{\nu}]) \mathbf{e}_\beta = \begin{cases} (1 + (\partial_\mu h)^2)^{-1} (\partial_k h)(\partial_\alpha \partial_\beta h), & \text{if } 1 \leq k \leq 2, \\ - (1 + (\partial_\mu h)^2)^{-1} (\partial_\alpha \partial_\beta h), & \text{if } k = 3. \end{cases}$$

448 Thus, for each  $k = 1, 2, 3$ ,

$$449 \quad (5.9) \quad \mathbf{e}_\alpha^T \left( \nu^k [\nabla_\Gamma \boldsymbol{\nu}] + \nabla_\Gamma \nabla_\Gamma \text{id}_\Gamma^k \right) \mathbf{e}_\beta = 0, \quad \text{for } 1 \leq \alpha, \beta \leq 2.$$

450 Since  $\{\mathbf{e}_1, \mathbf{e}_2\}$  spans the tangent space, and both  $\nabla_\Gamma \boldsymbol{\nu}$  and  $\nabla_\Gamma \nabla_\Gamma \text{id}_\Gamma^k$  are tangential  
451 tensors, we obtain (5.1).  $\square$

452 **5.2. The Scheme.** The first step in the method is to approximate the surface  
453 Hessian of  $\text{id}_\Gamma$ . For the convergence analysis, we assume  $\Gamma$  is  $C^{r+3}$ , where  $r \geq 0$  is  
454 the degree of the HHJ space. This implies that  $\text{id}_\Gamma \in [W^{r+3, \infty}(\Gamma)]^3$ , which means  
455  $\boldsymbol{\sigma}^k := \nabla_\Gamma \nabla_\Gamma \text{id}_\Gamma^k \in W^{r+1, \infty}(\Gamma; \mathbf{S})$ , for  $k = 1, 2, 3$ . Upon recalling (3.12), a direct  
456 calculation shows that

$$457 \quad (5.10) \quad a(\boldsymbol{\sigma}^k, \boldsymbol{\varphi}) + b_h(\boldsymbol{\varphi}, \text{id}_\Gamma^k) = \left( \boldsymbol{\varphi}^{\text{nn}}, \mathbf{n} \cdot \nabla_\Gamma \text{id}_\Gamma^k \right)_{\Sigma_c}, \quad \forall \boldsymbol{\varphi} \in \mathcal{V}_h, \quad \text{for } k = 1, 2, 3.$$

458 Thus, we take  $\text{id}_\Gamma^k$  as given data, and  $\boldsymbol{\sigma}^k$  is the  $L^2(\Gamma)$  projection of  $\nabla_\Gamma \nabla_\Gamma \text{id}_\Gamma^k$ . Indeed,  
459 (5.10) comes from replacing  $\boldsymbol{\sigma}$  in (3.12) with  $\boldsymbol{\sigma}^k$ , and replacing  $w, g$  with  $\text{id}_\Gamma^k$ . In  
460 addition, we have  $\boldsymbol{\rho}^k \in W^{r+1, \infty}(\Gamma; \mathbf{S})$ , such that the conormal-conormal moment  
461 satisfies  $\mathbf{n}^T \boldsymbol{\sigma}^k \mathbf{n} = \mathbf{n}^T \boldsymbol{\rho}^k \mathbf{n}$  on  $\Sigma_s$ .

462 The fully discrete method is as follows. Let  $\hat{\rho}_h^k$  be given by  $\hat{\rho}_h^k := B_h^m \tilde{\rho}^k$ , with  $\tilde{\rho}^k$   
 463 satisfying  $\rho^k \circ \Psi^m = \text{Piola}(\tilde{\rho}^k)$ , and  $B_h^m : H_h^0(\Gamma^m) \rightarrow V_h^m$  is the projection defined  
 464 by (4.10), which satisfies the following approximation properties:  $\|\hat{\rho}_h^k - \tilde{\rho}^k\|_{0,h,m} \leq$   
 465  $Ch^{r+1}\|\rho^k\|_{H^{r+1}(\Gamma)}$ , and  $\|\hat{\rho}_h^k - \tilde{\rho}^k\|_{L^\infty(\Sigma^m)} \leq Ch^{r+1}\|\rho^k\|_{W^{r+1,\infty}(\Gamma)}$  (c.f. [3, Supp.  
 466 Mater.: Sec. SM4.3]).

467 Then we let  $\hat{\sigma}_h^k = \hat{\sigma}_h^k + \hat{\rho}_h^k$ , and impose that  $\hat{\sigma}_h^k \in V_h^m$ , for  $k = 1, 2, 3$ , satisfies

$$468 \quad (5.11) \quad a^m(\hat{\sigma}_h^k, \hat{\varphi}_h) = -a^m(\hat{\rho}_h^k, \hat{\varphi}_h) - b_h^m(\hat{\varphi}_h, \text{id}_{\Gamma^m}^k) + (\hat{\varphi}_h^{\text{nn}}, \hat{\mathbf{n}} \cdot \tilde{\xi}^k)_{\Sigma_c^m},$$

469 for all  $\hat{\varphi}_h \in V_h^m$ , where  $\text{id}_{\Gamma^m}^k \in W_h^m$  and  $\tilde{\xi}^k := (\nabla_{\Gamma} \text{id}_{\Gamma^m}^k) \circ \Psi^m$ . Note that (5.11) is  
 470 simply (4.9) with  $\hat{\sigma}_h$  replaced with  $\hat{\sigma}_h^k$ ,  $\hat{\rho}_h$  replaced by  $\hat{\rho}_h^k$ ,  $\tilde{w}$  replaced by  $\text{id}_{\Gamma^m}^k$ , and  
 471  $\tilde{\xi}$  replaced by  $\tilde{\xi}^k$ . Similar to (4.13), we have that the discrete projection is stable:  
 472  $\|\hat{\sigma}_h^k\|_{0,h,m} \leq C(\|\hat{\rho}_h^k\|_{L^2(\Gamma^m)} + \|\nabla_{\Gamma} \text{id}_{\Gamma^m}^k\|_{L^2(\Gamma)})$ .

473 The last step in the method is to use (5.1), i.e. let  $\mathbf{S}_h$  approximate  $\nabla_{\Gamma} \nu$  through

$$474 \quad (5.12) \quad \mathbf{S}_h := -\hat{\nu}^k \hat{\sigma}_h^k \in L^2(\Gamma^m; \mathbf{S}^m),$$

475 where  $\hat{\nu} = (\hat{\nu}^1, \hat{\nu}^2, \hat{\nu}^3)$  is the unit normal vector of  $\Gamma^m$ . From (3.3), and the discussion  
 476 in subsection 3.1,  $\|\nu \circ \Psi^m - \hat{\nu}\|_{L^\infty(\Gamma^m)} \leq Ch^m$ . Then, by the error analysis of  
 477 subsection 4.5, and the triangle inequality, we obtain Theorem 5.2.

478 **THEOREM 5.2.** *Assume  $r \geq 0$  is the degree of  $V_h^m$  and that  $\Gamma$  is  $C^{r+3}$ . Moreover,*  
 479 *let  $\nabla_{\Gamma} \nu$  be the shape operator of  $\Gamma$ , and let  $\mathbf{S}_h$  be given by (5.12). If  $m \geq r + 1$ , then*

$$480 \quad (5.13) \quad \|\nabla_{\Gamma} \nu - \mathbf{S}_h \circ (\Psi^m)^{-1}\|_{L^2(\Gamma)} \leq Ch^{r+1},$$

481 where  $C > 0$  depends on the domain  $\Gamma$  and the shape regularity of the mesh.

482 **5.3. Practical Computation.** Usually, we choose  $m = r + 1$  when implement-  
 483 ing the method. For  $r = 0$ , this corresponds to piecewise linear surface triangulations  
 484 and piecewise linear Lagrange space, as well as a piecewise constant HHJ space.

485 **5.3.1. Closed Surfaces.** The method is simplest when posed on closed surface  
 486 triangulations. In this case,  $\hat{\rho}_h^k$  and  $\tilde{\xi}^k$  are unnecessary, so (5.11) reduces to the  
 487 following: find  $\hat{\sigma}_h^k \in V_h^m$ , for  $k = 1, 2, 3$ , such that

$$488 \quad (5.14) \quad a^m(\hat{\sigma}_h^k, \hat{\varphi}_h) = -b_h^m(\hat{\varphi}_h, \text{id}_{\Gamma^m}^k), \quad \forall \hat{\varphi}_h \in V_h^m.$$

489 The matrix representations of  $a^m(\cdot, \cdot)$  and  $b_h^m(\cdot, \cdot)$  are straightforward to assemble  
 490 using standard finite element software, even for  $m > 1$ , although the  $m = 1$  case is  
 491 especially simple. Indeed, the HHJ element, though not as well known as some other  
 492 elements, is implemented in several software packages, e.g. **FELICITY** [38], **FEniCS** [2],  
 493 **Firedrake** [32], **NGSolve** [36].

494 Let  $A^m$  and  $B^m$  be the matrix realizations of  $a^m(\cdot, \cdot)$  and  $b_h^m(\cdot, \cdot)$ , respectively.  
 495 Then the right-hand-side of (5.14) is simply  $-B^m X^k$ , where  $X^k$  is a column vector  
 496 containing the  $k$ th coordinate of the Degrees-of-Freedom of the Lagrange space  $W_h^m$ .  
 497 Let  $S^k$  be the coefficient vector corresponding to  $\hat{\sigma}_h^k$ . Then, one needs to solve the  
 498 linear system:  $A^m S^k = -B^m X^k$  for  $S^k$ , which is similar to computing a standard  $L^2$   
 499 projection.

500 However, the matrix  $A^m$  is slightly different from the usual mass matrix because  
 501 of the mesh dependent space  $H_h^0(\Gamma^m)$ , i.e. because of the edge terms. Effectively, this  
 502 causes the condition number of  $A^m$  to have a slight growth as the mesh size decreases.  
 503 See Table 1 for a listing of the condition number of  $A^m$  in the numerical experiments.

504 **5.3.2. Surfaces with Boundary.** Surfaces with boundary pose some difficulty,  
 505 because extra information about the surface is needed on the boundary  $\Sigma \equiv \partial\Gamma$ .  
 506 Applying the scheme (5.11) requires  $\tilde{\xi}^k = (\nabla_\Gamma \text{id}_\Gamma^k) \circ \Psi^m$  on  $\Sigma_c^m$ , which implies that  
 507 we need a good approximation of  $\nabla_\Gamma \text{id}_\Gamma \equiv \mathbf{P} = \mathbf{I} - \boldsymbol{\nu} \otimes \boldsymbol{\nu}$  on  $\Sigma_c$  or, equivalently, a  
 508 good approximation of  $\boldsymbol{\nu}$  on  $\Sigma_c$ . Thus, let  $\tilde{\boldsymbol{\nu}} \in [L^\infty(\Sigma_c^m)]^3$  with the property that

$$509 \quad (5.15) \quad \|\boldsymbol{\nu} - \tilde{\boldsymbol{\nu}} \circ (\Psi^m)^{-1}\|_{L^\infty(\Sigma_c)} = O(h^{m+1/2}).$$

510 Note that this precludes directly using the discrete normal  $\hat{\boldsymbol{\nu}}$  of  $\Gamma^m$ .

511 Next, we must account for boundary values on  $\Sigma_s$ . Let  $\boldsymbol{\rho}^k \in W^{r+1,\infty}(\Gamma; \mathbf{S})$ , be  
 512 given by  $\boldsymbol{\rho}^k := -\nu^k \nabla_\Gamma \boldsymbol{\nu} \equiv \boldsymbol{\sigma}^k$ , for  $k = 1, 2, 3$  (see (5.1)), and evaluate (4.10), i.e.  
 513 define  $\hat{\boldsymbol{\rho}}_h^k \in V_h^m$ , for  $k = 1, 2, 3$ , as the unique solution of

$$514 \quad (5.16) \quad (\hat{\boldsymbol{\rho}}_h^k - \tilde{\boldsymbol{\rho}}^k, \hat{\boldsymbol{\varphi}}_h)_{\mathcal{T}_h^m} + (\hat{\mathbf{n}}^T [\hat{\boldsymbol{\rho}}_h^k - \tilde{\boldsymbol{\rho}}^k] \hat{\mathbf{n}}, \hat{\varphi}_h^{\text{nn}})_{\mathcal{E}_h^m} = 0, \quad \forall \hat{\boldsymbol{\varphi}}_h \in V_h^m,$$

515 where  $\hat{\mathbf{n}}$  is the co-normal vector on  $\Sigma_s^m$  and  $\tilde{\boldsymbol{\rho}}^k$  is given by  $\boldsymbol{\rho}^k \circ \Psi^m = \tilde{\boldsymbol{\rho}}^k$ . Then use  
 516  $\hat{\boldsymbol{\rho}}_h^k$  to enforce boundary conditions on  $\hat{\boldsymbol{\sigma}}_h^k$ . However, for solving the discrete problem  
 517 (5.11), we only need the values of  $\hat{\boldsymbol{\rho}}_h^k$  on  $\Sigma_s^m$ . Ergo, we can restrict (5.16) to a  
 518 boundary integral on  $\Sigma_s^m$ . Furthermore, we can utilize a good approximation of the  
 519 boundary curvature in the following sense. Let  $\tilde{\kappa}_h^n \in L^\infty(\Sigma_s^m)$  be an approximation  
 520 of the *normal curvature*, in the co-normal direction  $\mathbf{n}$ , with the property that

$$521 \quad (5.17) \quad \|\mathbf{n}^T [\nabla_\Gamma \boldsymbol{\nu}] \mathbf{n} - \tilde{\kappa}_h^n \circ (\Psi^m)^{-1}\|_{L^\infty(\Sigma_s)} = O(h^m).$$

522 Then, we define  $\hat{\boldsymbol{\rho}}_h^k \in V_h^m$ , for  $k = 1, 2, 3$ , as the unique solution of

$$523 \quad (5.18) \quad (\hat{\mathbf{n}}^T \hat{\boldsymbol{\rho}}_h^k \hat{\mathbf{n}}, \hat{\mathbf{n}}^T \hat{\boldsymbol{\varphi}}_h \hat{\mathbf{n}})_{\Sigma_s^m} = -(\hat{\nu}^k \tilde{\kappa}_h^n, \hat{\mathbf{n}}^T \hat{\boldsymbol{\varphi}}_h \hat{\mathbf{n}})_{\Sigma_s^m}, \quad \forall \hat{\boldsymbol{\varphi}}_h \in V_h^m,$$

524 where we use the discrete normal  $\hat{\boldsymbol{\nu}}$  of  $\Gamma^m$  and we set all degrees-of-freedom (DoFs) of  
 525  $\hat{\boldsymbol{\rho}}_h^k$  not on  $\Sigma_s^m$  to zero. Note that the matrix realization of the left-hand-side of (5.18)  
 526 is block diagonal, where each block corresponds to an edge of  $\Sigma_s^m$ ; hence, (5.18) is a  
 527 trivial linear system to solve.

528 We now summarize the method. Let  $\hat{\boldsymbol{\rho}}_h^k$  be given by (5.18) and  $\tilde{\boldsymbol{\nu}}$  satisfy (5.15).  
 529 Then, find  $\hat{\boldsymbol{\sigma}}_h^k \in V_h^m$ , for  $k = 1, 2, 3$ , such that

$$530 \quad (5.19) \quad a^m(\hat{\boldsymbol{\sigma}}_h^k, \hat{\boldsymbol{\varphi}}_h) = -a^m(\hat{\boldsymbol{\rho}}_h^k, \hat{\boldsymbol{\varphi}}_h) - b_h^m(\hat{\boldsymbol{\varphi}}_h, \text{id}_{\Gamma^m}^k) + (\hat{\varphi}_h^{\text{nn}}, \hat{\mathbf{n}}^k - (\hat{\mathbf{n}} \cdot \tilde{\boldsymbol{\nu}}) \hat{\nu}^k)_{\Sigma_c^m},$$

531 for all  $\hat{\boldsymbol{\varphi}}_h \in V_h^m$ . Then, set  $\hat{\boldsymbol{\sigma}}_h^k := \hat{\boldsymbol{\sigma}}_h^k + \hat{\boldsymbol{\rho}}_h^k$  and define  $\mathbf{S}_h := -\hat{\nu}^k \hat{\boldsymbol{\sigma}}_h^k$ .

532 **THEOREM 5.3.** *Adopt the hypothesis of Theorem 5.2, but let  $\mathbf{S}_h$  be computed by*  
 533 *the scheme in (5.19). If  $m \geq r + 1$ , then*

$$534 \quad (5.20) \quad \|\nabla_\Gamma \boldsymbol{\nu} - \mathbf{S}_h \circ (\Psi^m)^{-1}\|_{L^2(\Gamma)} \leq Ch^{r+1},$$

535 where  $C > 0$  depends on the domain  $\Gamma$  and the shape regularity of the mesh.

536 Note that, by the properties of the projection and the HHJ interpolant (see sub-  
 537 section 4.2), we have  $\|\hat{\boldsymbol{\rho}}_h^k - \tilde{\boldsymbol{\rho}}^k\|_{L^\infty(\Sigma^m)} \leq Ch^{r+1} \|\boldsymbol{\rho}^k\|_{W^{r+1,\infty}(\Gamma)}$  (c.f. [3, Supp. Mater.:  
 538 Sec. SM4.3]).

539 *Remark 5.4.* The partition of the boundary,  $\Sigma = \overline{\Sigma_c} \cup \overline{\Sigma_s}$ , depends on the geo-  
 540 metric information available at the boundary. One can have  $\Sigma \equiv \Sigma_c$ , or  $\Sigma \equiv \Sigma_s$ , or a  
 541 combination, so the method has some flexibility.

542 **6. Numerical Results.** We present numerical results for several different do-  
 543 mains, both with and without boundary. The discrete domains were generated by  
 544 either interpolating charts on a sequence of uniformly refined grids, or by creating an  
 545 initial piecewise linear triangulation of the implicit, closed surface (using [37]) and  
 546 interpolating the closest point map. As above, the finite element spaces  $V_h$  and  $W_h$   
 547 are of degree  $r$  and  $r + 1$  respectively, where  $r \geq 0$ , and the geometric approximation  
 548 degree is denoted  $m$ , and satisfies  $m = r + 1$ . All computations were done with the  
 549 Matlab/C++ finite element toolbox FELICITY [38], where we used the “backslash”  
 550 command in Matlab to solve the linear systems.

551 From (4.14), recall that  $\mathbf{F}^m := \mathcal{I}_h^{1,m} \Psi^1$ , which is possible to implement, but  
 552 inconvenient. Instead, we first compute  $\mathbf{F}^{m+1}$  by standard nodal interpolation, then  
 553 we define  $\mathbf{F}^m := \mathcal{I}_h^{1,m} \mathbf{F}^{m+1}$ , which is easy to implement over the piecewise linear  
 554 triangulation of  $\Gamma^1$  and does not affect the accuracy.

555 As for the boundary data,  $\nu$  and  $\nabla_\Gamma \nu$  are known through the exact surface  
 556 geometry. Moreover, these functions are easily extended away from the surface by  
 557 analytic continuation. Thus, we use  $\tilde{\nu} := I_h^m \nu$  and  $\tilde{\kappa}_h^n := \hat{\mathbf{n}}^T (I_h^m [\nabla_\Gamma \nu]) \hat{\mathbf{n}}$ , where  
 558  $I_h^m : H_h^2(\Gamma^m) \rightarrow W_h^m$  (different from  $\mathcal{I}_h^m$ ) is the standard, pointwise, nodal interpolant  
 559 onto  $W_h^m$ . Note: when  $m = 1$ , then  $I_h^1 \equiv \mathcal{I}_h^{1,1}$ .

560 In order to illustrate the effectiveness of the method, we compute the following  
 561 errors:  $\|I_h^m(\nu \circ \Psi^m) - \tilde{\nu}\|_{L^2(\Gamma^m)}$ ,  $\|I_h^m[(\nabla_\Gamma \nu) \circ \Psi^m] - \mathbf{S}_h\|_{L^2(\Gamma^m)}$ ,  $\|I_h^m[(\nabla_\Gamma \nu) \circ \Psi^m] - \mathbf{S}_h\|_{L^\infty(\Gamma^m)}$ ,  
 562  $\|I_h^m(\kappa^a \circ \Psi^m) - \kappa_h^a\|_{L^2(\Gamma^m)}$ ,  $\|I_h^m(\kappa^g \circ \Psi^m) - \kappa_h^g\|_{L^2(\Gamma^m)}$ , where  $\kappa^a = \kappa^1 + \kappa^2$   
 563 (additive curvature),  $\kappa^g = \kappa^1 \cdot \kappa^2$  (Gauss curvature), and

$$564 \quad (6.1) \quad \kappa_h^a := \text{tr } \mathbf{S}_h, \quad \kappa_h^g := \det [\mathbf{S}_h + \hat{\nu} \otimes \hat{\nu}].$$

565 Again, the geometric information is extended away from the surface by analytic con-  
 566 tinuation. These errors can be related to the ones in (5.13), (5.20) by equivalence  
 567 of norms and a triangle inequality. The estimated order of convergence (EOC) is  
 568 computed by using the ratio of the error between two successive uniform refinements.

569 In order to avoid spurious results in the numerical convergence tests, the meshes  
 570 in the examples were generated from the non-uniform/non-symmetric meshes shown  
 571 in Figure 2. The condition numbers of the “mass” matrix to invert in projecting to  
 572 the HHJ space are listed in Table 1.

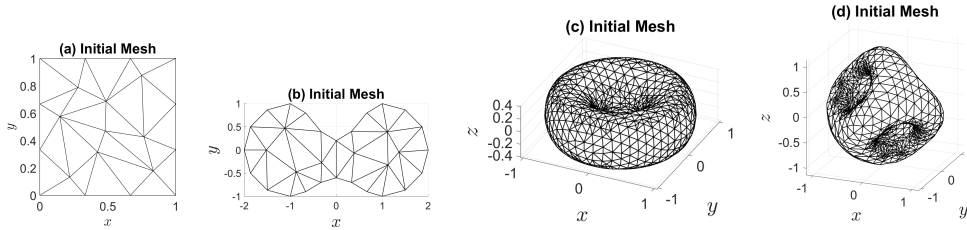


FIG. 2. All initial meshes. (a,b) These meshes are uniformly refined twice to give the  $k = 0$  case in Table 2, Table 3; (c,d) These meshes correspond to the  $k = 0$  case in Table 4, Table 5.

573 **6.1. Saddle Surface on a Square.** The domain is given by  $(U, \chi)$ , where  
 574  $U = [0, 1] \times [0, 1]$  is the unit square and  $\chi(u^1, u^2) = (u^1, u^2, 0.5(\sin(3.5(u^1 - 0.5)) + \cos(4.2(u^2 - 0.5))))$ . Figure 3 shows the surface with curvature data obtained from  
 575



TABLE 1

Listing of the 2-norm condition number of the matrix  $A^m$  discussed in subsection 5.3.1. Numbers correspond to the convergence tables in the associated sections for  $m = 1$ ; for  $m = 2, 3$ , the condition numbers were larger by factors of approximately  $10^2$  and  $10^3$ , respectively. The number in parenthesis is the condition number of  $(D^m)^{-1}A^m$ , where  $D^m$  is a diagonal matrix obtained by mass-lumping of  $A^m$ .

$k$	subsection 6.1	subsection 6.2	subsection 6.3	subsection 6.4
0	7.61E02 (4.89E02)	3.90E02 (1.80E02)	2.89E02 (2.15E01)	4.39E02 (3.13E01)
1	9.65E02 (6.93E02)	4.87E02 (2.41E02)	4.55E02 (3.80E01)	7.10E02 (6.23E01)
2	1.11E03 (8.93E02)	5.69E02 (3.04E02)	5.88E02 (5.42E01)	8.75E02 (1.01E02)
3	1.18E03 (1.05E03)	6.39E02 (3.62E02)	7.00E02 (6.74E01)	9.64E02 (1.31E02)
4	1.26E03 (1.15E03)	6.95E02 (4.05E02)	7.72E02 (7.57E01)	1.00E03 (1.53E02)

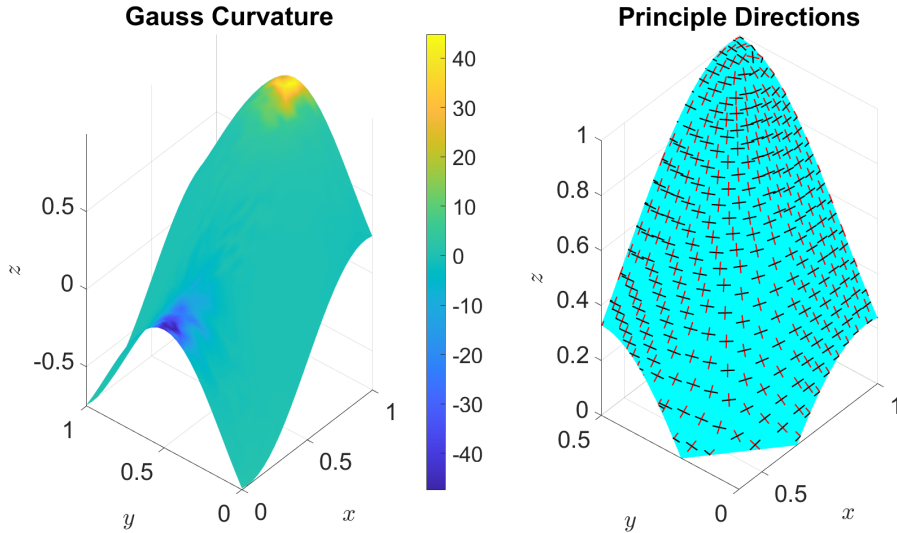


FIG. 3. Illustration of the saddle surface in subsection 6.1 corresponding to  $m = 1$  and  $k = 1$  in Table 2. Left: color corresponds to the discrete Gauss curvature  $\kappa_h^g$ . Right: zoom-in of the surface where line segments indicate the principle directions of the surface, i.e. red (black) is  $\mathbf{d}_1$  ( $\mathbf{d}_2$ ), which correspond to the minimum (maximum) curvature direction.

576 the discrete approximation. Table 2 shows the convergence behavior for the case of  
 577 clamped boundary data (i.e. using  $\tilde{\nu}$ ), which confirms the error estimate in (5.20).

578 **6.2. Wavy Dumbbell.** The domain is given by  $(U, \chi)$ , where the boundary of  
 579  $U$  is piecewise parametrized by

$$(6.2) \quad (x(t), y(t)) = \begin{cases} (\cos(t) + 1, \sin(t)), & \text{if } -\pi/2 \leq t \leq \pi/2, \\ (-t + 1, 0.6 + 0.4 \cos(\pi t)), & \text{if } 0 \leq t \leq 2, \\ (\cos(t) - 1, \sin(t)), & \text{if } \pi/2 \leq t \leq 3\pi/2, \\ (t - 1, -(0.8 + 0.2 \cos(\pi t))), & \text{if } 0 \leq t \leq 2. \end{cases}$$

581 The surface parametrization is given by  $\chi(u, v) = (u, v, e^{-u^2} \sin(2v))$ . The curved  
 582 element mapping is composed from two maps (recall (4.14)). The first map is a Lenoir  
 583 type map, [26] described in [3] that creates a curved triangulation that optimally  
 584 approximates  $U$ ; the second map is the parametrization  $\chi$ . We then apply (4.14) to

TABLE 2

Convergence errors for the saddle surface (subsection 6.1) using clamped boundary data; EOC is shown in parenthesis. The number of triangles in the mesh is  $N_T = 448 \cdot 4^k$ , where  $k$  is the refinement index. Cases are shown for  $m = 1, 2, 3$ , where  $m$  is the polynomial degree of the geometry.

$k$	$L^2$ error: $\nu$	$L^2$ error: $\nabla_{\Gamma}\nu$	$L^\infty$ error: $\nabla_{\Gamma}\nu$	$L^2$ error: $\kappa^a$	$L^2$ error: $\kappa^g$
$m = 1$ :					
0	1.09E-01 (1.02)	1.04E 00 (0.84)	1.13E 00 (1.77)	5.94E-01 (0.89)	2.48E 00 (1.02)
1	5.44E-02 (1.01)	5.48E-01 (0.92)	4.45E-01 (1.35)	3.09E-01 (0.94)	1.26E 00 (0.97)
2	2.72E-02 (1.00)	2.81E-01 (0.96)	2.31E-01 (0.95)	1.57E-01 (0.97)	6.44E-01 (0.97)
3	1.36E-02 (1.00)	1.42E-01 (0.98)	1.27E-01 (0.86)	7.97E-02 (0.98)	3.26E-01 (0.98)
4	6.79E-03 (1.00)	7.15E-02 (0.99)	6.65E-02 (0.94)	4.02E-02 (0.99)	1.64E-01 (0.99)
$m = 2$ :					
0	3.87E-03 (2.19)	1.52E-01 (1.87)	8.89E-01 (0.94)	9.77E-02 (1.78)	4.69E-01 (1.57)
1	9.13E-04 (2.08)	3.71E-02 (2.03)	2.83E-01 (1.65)	2.49E-02 (1.97)	1.23E-01 (1.93)
2	2.25E-04 (2.02)	9.07E-03 (2.03)	8.35E-02 (1.76)	6.10E-03 (2.03)	3.08E-02 (2.00)
3	5.59E-05 (2.01)	2.25E-03 (2.01)	2.14E-02 (1.96)	1.51E-03 (2.01)	7.68E-03 (2.00)
4	1.40E-05 (2.00)	5.62E-04 (2.00)	5.41E-03 (1.99)	3.77E-04 (2.00)	1.92E-03 (2.00)
$m = 3$ :					
0	1.20E-04 (3.51)	1.41E-02 (2.95)	2.00E-01 (2.56)	1.08E-02 (2.72)	5.10E-02 (2.81)
1	1.15E-05 (3.38)	1.86E-03 (2.93)	2.12E-02 (3.24)	1.50E-03 (2.85)	7.47E-03 (2.77)
2	1.28E-06 (3.16)	2.37E-04 (2.97)	1.77E-03 (3.58)	1.92E-04 (2.97)	9.68E-04 (2.95)
3	1.55E-07 (3.05)	2.98E-05 (2.99)	2.20E-04 (3.01)	2.42E-05 (2.99)	1.22E-04 (2.99)
4	1.92E-08 (3.01)	3.73E-06 (3.00)	2.73E-05 (3.01)	3.03E-06 (3.00)	1.53E-05 (3.00)

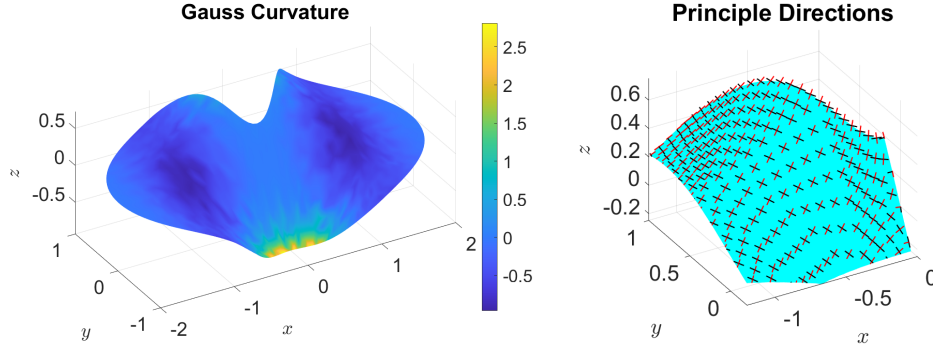


FIG. 4. Illustration of the wavy dumbbell in subsection 6.2 corresponding to  $m = 1$  and  $k = 1$  in Table 3. The format is similar to Figure 3. Right figure is zoomed in on the top, curved edge of the surface.

585 the composed map.

586 Figure 4 shows the surface with curvature data obtained from the discrete ap-  
 587 proximation. Table 3 shows the convergence behavior for the case of simply-supported  
 588 boundary data (i.e. using  $\tilde{\kappa}_h^n$ ), which confirms the error estimate in (5.20).

589 **6.3. Torus.** The domain is a torus described by the zero level set of the function:  
 590  $b(x, y, z) = (x^2 + y^2 - (6/10))^2 + (3/2)z^2 - (1/4)$ . The parameterization is built from  
 591 the closest point map. Figure 5 shows the surface with curvature data obtained from  
 592 the discrete approximation. Table 4 shows the convergence behavior, which confirms  
 593 the error estimate in (5.13).

TABLE 3

Convergence errors for the wavy dumbbell (subsection 6.2) using simply-supported boundary data (similar format as Table 2). The number of triangles in the mesh is  $N_T = 608 \cdot 4^k$ , where  $k$  is the refinement index.

$k$	$\ \nu_h\ _{L^2}$	$\ \mathcal{S}_h\ _{L^2}$	$\ \mathcal{S}_h\ _{L^\infty}$	$\ H_h\ _{L^2}$	$\ K_h\ _{L^2}$
$m = 1$ :					
0	1.65E-01 (1.00)	5.62E-01 (0.95)	4.37E-01 (1.01)	3.67E-01 (1.01)	4.05E-01 (1.01)
1	8.25E-02 (1.00)	2.86E-01 (0.97)	2.13E-01 (1.04)	1.84E-01 (1.00)	2.05E-01 (0.98)
2	4.12E-02 (1.00)	1.44E-01 (0.99)	1.00E-01 (1.09)	9.22E-02 (1.00)	1.04E-01 (0.98)
3	2.06E-02 (1.00)	7.23E-02 (0.99)	4.79E-02 (1.06)	4.63E-02 (1.00)	5.22E-02 (0.99)
4	1.03E-02 (1.00)	3.62E-02 (1.00)	2.33E-02 (1.04)	2.32E-02 (1.00)	2.62E-02 (1.00)
$m = 2$ :					
0	8.31E-03 (2.00)	3.79E-02 (1.99)	1.08E-01 (1.62)	2.35E-02 (2.04)	2.81E-02 (2.00)
1	2.07E-03 (2.01)	9.41E-03 (2.01)	2.78E-02 (1.95)	5.68E-03 (2.05)	6.95E-03 (2.01)
2	5.16E-04 (2.00)	2.34E-03 (2.01)	6.60E-03 (2.08)	1.39E-03 (2.03)	1.73E-03 (2.01)
3	1.29E-04 (2.00)	5.83E-04 (2.00)	1.55E-03 (2.09)	3.45E-04 (2.01)	4.30E-04 (2.01)
4	3.22E-05 (2.00)	1.46E-04 (2.00)	3.69E-04 (2.07)	8.59E-05 (2.01)	1.07E-04 (2.00)
$m = 3$ :					
0	3.92E-04 (3.04)	3.78E-03 (2.83)	1.30E-02 (2.42)	2.12E-03 (2.72)	2.64E-03 (2.84)
1	4.85E-05 (3.02)	4.94E-04 (2.93)	2.26E-03 (2.53)	2.95E-04 (2.85)	3.49E-04 (2.92)
2	6.04E-06 (3.01)	6.28E-05 (2.98)	3.29E-04 (2.78)	3.83E-05 (2.94)	4.46E-05 (2.97)
3	7.53E-07 (3.00)	7.88E-06 (2.99)	4.42E-05 (2.89)	4.85E-06 (2.98)	5.60E-06 (2.99)
4	9.41E-08 (3.00)	9.87E-07 (3.00)	5.72E-06 (2.95)	6.09E-07 (2.99)	7.01E-07 (3.00)

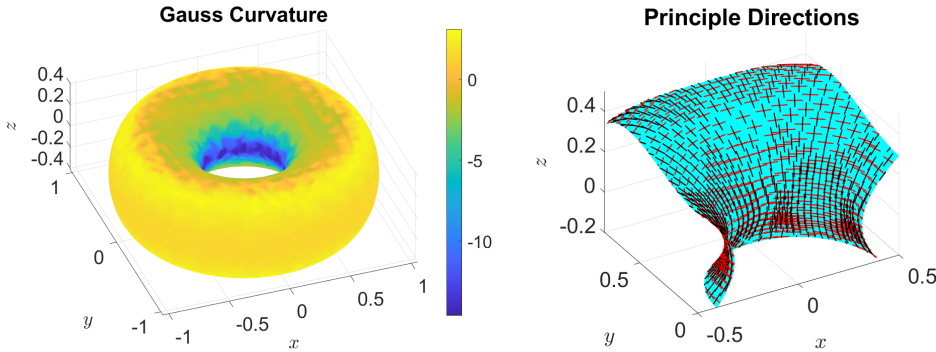


FIG. 5. Illustration of the torus in subsection 6.3 corresponding to  $m = 1$  and  $k = 1$  in Table 4. The format is similar to Figure 3. Right figure is zoomed in on the inner hole region.

594 **6.4. A Genus-3 Surface.** The domain is closed surface described by the zero  
595 level set of the function:

$$\begin{aligned}
 (6.3) \quad b(x, y, z) = & (a_0x - 2)^2(a_0x + 2)^2 + (a_0y - 2)^2(a_0y + 2)^2 \\
 & + (a_0z - 2)^2(a_0z + 2)^2 + 3a_0^4(x^2y^2 + x^2z^2 + y^2z^2) \\
 & + 6a_0^3xyz - 10a_0^2(x^2 + y^2 + z^2) + 11.5,
 \end{aligned}$$

597 where  $a_0 = 3.25$ . The parameterization is built from the closest point map. Figure 6  
598 shows the surface with curvature data obtained from the discrete approximation.  
599 Table 5 shows the convergence behavior, which confirms the error estimate in (5.13).

600 **7. Conclusion.** We have presented an effective finite element technique that can  
601 post-process a scalar Lagrange finite element function on a discrete surface to produce  
602 an accurate approximation of the surface Hessian of the function. The method is  
603 straightforward and does not require any ad-hoc modifications. Furthermore, the

TABLE 4

Convergence errors for the torus (subsection 6.3) (similar format as Table 2). The number of triangles in the mesh is  $N_T = 1904 \cdot 4^k$ , where  $k$  is the refinement index.

$k$	$\ \nu_h\ _{L^2}$	$\ S_h\ _{L^2}$	$\ S_h\ _{L^\infty}$	$\ H_h\ _{L^2}$	$\ K_h\ _{L^2}$
$m = 1$ :					
0	3.16E-01 (0.00)	2.03E 00 (0.00)	6.05E-01 (0.00)	1.05E 00 (0.00)	2.55E 00 (0.00)
1	1.59E-01 (1.00)	1.07E 00 (0.92)	3.80E-01 (0.67)	5.58E-01 (0.91)	1.41E 00 (0.85)
2	7.93E-02 (1.00)	5.54E-01 (0.96)	1.81E-01 (1.07)	2.97E-01 (0.91)	7.54E-01 (0.91)
3	3.97E-02 (1.00)	2.81E-01 (0.98)	1.01E-01 (0.84)	1.56E-01 (0.94)	3.90E-01 (0.95)
4	1.98E-02 (1.00)	1.42E-01 (0.99)	5.25E-02 (0.94)	7.98E-02 (0.96)	1.99E-01 (0.97)
$m = 2$ :					
0	1.76E-02 (0.00)	1.98E-01 (0.00)	3.24E-01 (0.00)	1.60E-01 (0.00)	3.70E-01 (0.00)
1	4.35E-03 (2.00)	4.94E-02 (2.00)	1.04E-01 (1.64)	4.21E-02 (1.93)	9.95E-02 (1.89)
2	1.08E-03 (2.00)	1.23E-02 (2.01)	3.29E-02 (1.66)	1.06E-02 (1.98)	2.58E-02 (1.95)
3	2.71E-04 (2.00)	3.08E-03 (2.00)	8.54E-03 (1.95)	2.67E-03 (1.99)	6.54E-03 (1.98)
$m = 3$ :					
0	5.06E-03 (0.00)	3.96E-02 (0.00)	5.69E-02 (0.00)	2.82E-02 (0.00)	5.79E-02 (0.00)
1	6.64E-04 (2.93)	5.12E-03 (2.95)	1.10E-02 (2.38)	3.64E-03 (2.96)	6.77E-03 (3.10)
2	8.38E-05 (2.99)	6.46E-04 (2.99)	1.63E-03 (2.75)	4.60E-04 (2.99)	8.30E-04 (3.03)
3	1.05E-05 (3.00)	8.10E-05 (2.99)	2.14E-04 (2.93)	5.78E-05 (2.99)	1.03E-04 (3.01)

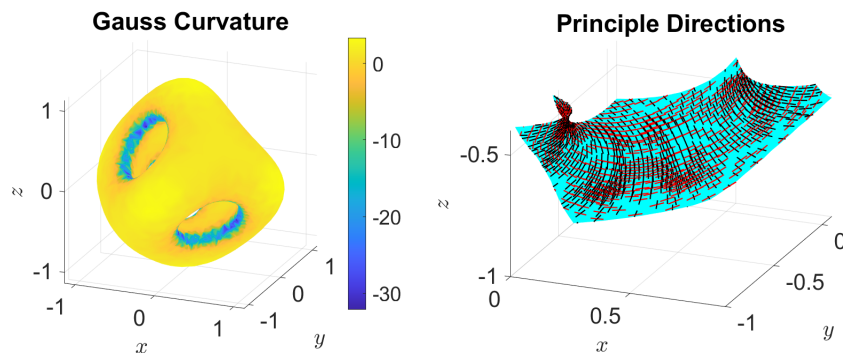


FIG. 6. Illustration of the genus-3 surface in subsection 6.4 corresponding to  $m = 1$  and  $k = 1$  in Table 5. The format is similar to Figure 3. Right figure is zoomed in on the edge of the right hole.

604 method is directly applicable to computing convergent approximations of the full  
 605 shape operator of the underlying surface (even piecewise linear triangulations) by  
 606 setting the scalar function to the identity map of the discrete surface.

607 An important aspect of our scheme is that it solves a global problem when com-  
 608 puting the projection onto an HHJ element, which is contrary to the methods in  
 609 [29, 20, 42] that compute the mean and gauss curvature of discrete surfaces (at a  
 610 vertex) using the 1-ring neighborhood of that vertex. Our scheme is convergent for  
 611 general meshes, whereas these purely local schemes are not. This also implies that one  
 612 should use an iterative method when solving the HHJ projection, including precon-  
 613 ditioning to account for the small growth in the condition number of the HHJ mass  
 614 matrix (see Table 1). Finding effective preconditioners is a point of future work.

615

## REFERENCES

- 616 [1] R. A. ADAMS AND J. J. F. FOURNIER, *Sobolev Spaces*, vol. 140 of Pure and Applied Mathematics  
 617 Series, Elsevier, 2nd ed., 2003.

TABLE 5

Convergence errors for the genus-3 surface (subsection 6.4) (similar format as Table 2). The number of triangles in the mesh is  $N_T = 2808 \cdot 4^k$ , where  $k$  is the refinement index.

$k$	$\ \nu_h\ _{L^2}$	$\ S_h\ _{L^2}$	$\ S_h\ _{L^\infty}$	$\ H_h\ _{L^2}$	$\ K_h\ _{L^2}$
$m = 1$ :					
0	5.77E-01 (0.00)	4.44E 00 (0.00)	2.06E 00 (0.00)	1.88E 00 (0.00)	9.14E 00 (0.00)
1	2.93E-01 (0.98)	2.39E 00 (0.89)	1.04E 00 (0.99)	1.15E 00 (0.72)	4.79E 00 (0.93)
2	1.47E-01 (0.99)	1.24E 00 (0.95)	5.95E-01 (0.80)	6.46E-01 (0.83)	2.62E 00 (0.87)
3	7.36E-02 (1.00)	6.34E-01 (0.97)	2.95E-01 (1.01)	3.44E-01 (0.91)	1.39E 00 (0.91)
4	3.68E-02 (1.00)	3.20E-01 (0.99)	1.42E-01 (1.06)	1.78E-01 (0.95)	7.12E-01 (0.97)
5	1.84E-02 (1.00)	1.61E-01 (0.99)	7.00E-02 (1.02)	9.03E-02 (0.98)	3.58E-01 (0.99)
$m = 2$ :					
0	4.37E-02 (0.00)	1.35E 00 (0.00)	2.43E 00 (0.00)	1.13E 00 (0.00)	7.05E 00 (0.00)
1	1.14E-02 (1.94)	3.51E-01 (1.94)	7.41E-01 (1.71)	2.77E-01 (2.02)	1.73E 00 (2.03)
2	2.85E-03 (2.00)	8.74E-02 (2.01)	2.58E-01 (1.52)	6.70E-02 (2.05)	4.19E-01 (2.04)
3	7.14E-04 (2.00)	2.17E-02 (2.01)	7.10E-02 (1.86)	1.63E-02 (2.04)	1.02E-01 (2.03)
4	1.78E-04 (2.00)	5.42E-03 (2.00)	2.05E-02 (1.79)	4.02E-03 (2.02)	2.53E-02 (2.02)
$m = 3$ :					
0	3.36E-02 (0.00)	6.03E-01 (0.00)	1.16E 00 (0.00)	3.84E-01 (0.00)	2.14E 00 (0.00)
1	4.23E-03 (2.99)	6.44E-02 (3.23)	1.74E-01 (2.75)	3.76E-02 (3.35)	2.22E-01 (3.27)
2	5.36E-04 (2.98)	7.54E-03 (3.09)	2.07E-02 (3.07)	4.48E-03 (3.07)	2.19E-02 (3.35)
3	6.73E-05 (2.99)	9.24E-04 (3.03)	2.66E-03 (2.96)	5.53E-04 (3.02)	2.37E-03 (3.21)

- 618 [2] M. ALNÆS, J. BLECHTA, J. HAKE, A. JOHANSSON, B. KEHLET, A. LOGG, C. RICHARDSON,  
619 J. RING, M. ROGNES, AND G. WELLS, *The fenics project version 1.5*, Archive of Numerical  
620 Software, 3 (2015), <https://doi.org/10.11588/ans.2015.100.20553>, <http://journals.uni-heidelberg.de/index.php/ans/article/view/20553>.
- 622 [3] D. N. ARNOLD AND S. W. WALKER, *The hellan–herrmann–johnson method with curved ele-*  
623 *ments*, SIAM Journal on Numerical Analysis, 58 (2020), pp. 2829–2855, [https://doi.org/](https://doi.org/10.1137/19M1288723)  
624 [10.1137/19M1288723](https://doi.org/10.1137/19M1288723), <https://arxiv.org/abs/https://doi.org/10.1137/19M1288723>.
- 626 [4] ARNOLD, D. N. AND BREZZI, F., *Mixed and nonconforming finite element methods : imple-*  
627 *mentation, postprocessing and error estimates*, ESAIM: M2AN, 19 (1985), pp. 7–32, [https://doi.org/](https://doi.org/10.1051/m2an/1985190100071)  
628 [10.1051/m2an/1985190100071](https://doi.org/10.1051/m2an/1985190100071).
- 629 [5] I. BABUŠKA, J. OSBORN, AND J. PITKÁRANTA, *Analysis of mixed methods using mesh dependent*  
630 *norms*, Mathematics of Computation, 35 (1980), pp. 1039–1062, [http://www.jstor.org/](http://www.jstor.org/stable/2006374)  
631 [stable/2006374](http://www.jstor.org/stable/2006374).
- 632 [6] A. BAC, J.-L. MARI, D. KUDELSKI, N.-V. TRAN, S. VISEUR, AND M. DANIEL, *Application*  
633 *of discrete curvatures to surface mesh simplification and feature line extraction*, Actes  
634 des rencontres du CIRM, 3 (2013), pp. 31–49, <https://doi.org/10.5802/acirm.53>, <https://acirm.centre-mersenne.org/articles/10.5802/acirm.53/>.
- 636 [7] U. BAUER, K. POLTHIER, AND M. WARDETZKY, *Uniform convergence of discrete curvatures*  
637 *from nets of curvature lines*, Discrete & Computational Geometry, 43 (2010), pp. 798–823,  
638 <https://doi.org/10.1007/s00454-009-9237-4>, <https://doi.org/10.1007/s00454-009-9237-4>.
- 639 [8] H. BLUM AND R. RANNACHER, *On mixed finite element methods in plate bending analysis.*  
640 *part 1: The first herrmann scheme*, Computational Mechanics, 6 (1990), pp. 221–236,  
641 <https://doi.org/10.1007/BF00350239>, <https://doi.org/10.1007/BF00350239>.
- 642 [9] A. I. BOBENKO AND B. A. SPRINGBORN, *A discrete laplace–beltrami operator for simplicial*  
643 *surfaces*, Discrete and Computational Geometry, 38 (2007), pp. 740–756, [https://doi.org/](https://doi.org/10.1007/s00454-007-9006-1)  
644 [10.1007/s00454-007-9006-1](https://doi.org/10.1007/s00454-007-9006-1).
- 645 [10] F. BREZZI AND P. A. RAVIART, *Mixed finite element methods for 4th order elliptic equations*,  
646 in Topics In Numerical Analysis III: Proceedings of the Royal Irish Academy Conference  
647 on Numerical Analysis, J. J. H. Miller, ed., Academic Press, 1976, pp. 33–56.
- 648 [11] P. G. CIARLET, *The Finite Element Method for Elliptic Problems*, Classics in Applied Mathe-  
649 matics, SIAM, Philadelphia, PA, 2nd ed., 2002. ISBN: 978-0898715149.
- 650 [12] A. DEMLOW, *Higher-order finite element methods and pointwise error estimates for elliptic*  
651 *problems on surfaces*, SIAM Journal on Numerical Analysis, 47 (2009), pp. 805–827, <https://doi.org/10.1137/070708135>, <https://doi.org/10.1137/070708135>, [https://arxiv.org/abs/](https://arxiv.org/abs/https://doi.org/10.1137/070708135)  
652 <https://doi.org/10.1137/070708135>, <https://doi.org/10.1137/070708135>.
- 653 [13] A. DEMLOW AND G. DZIUK, *An adaptive finite element method for the laplace–beltrami operator*  
654

- 655 *on implicitly defined surfaces*, SIAM Journal on Numerical Analysis, 45 (2007), pp. 421–  
656 442, <https://doi.org/10.1137/050642873>, [https://](https://doi.org/10.1137/050642873)  
657 [arxiv.org/abs/https://doi.org/10.1137/050642873](https://arxiv.org/abs/https://doi.org/10.1137/050642873).
- [14] M. DESBRUN, M. MEYER, P. SCHRÖDER, AND A. H. BARR, *Implicit fairing of irregular meshes*  
659 *using diffusion and curvature flow*, in SIGGRAPH '99: Proceedings of the 26th annual  
660 conference on Computer graphics and interactive techniques, New York, NY, USA, 1999,  
661 ACM Press/Addison-Wesley Publishing Co., pp. 317–324, [https://doi.org/10.1145/311535.](https://doi.org/10.1145/311535.311576)  
662 311576.
- [15] G. DZIUK, In *S. Hildebrandt, R. Leis (eds): Partial Differential Equations and Calculus of*  
664 *Variations*, vol. 1357, Springer, Berlin, Heidelberg, 1988, ch. Finite Elements For the Bel-  
665 trami Operator On Arbitrary Surfaces, pp. 142–155, <https://doi.org/10.1007/BFb0082865>.
- [16] G. DZIUK, *An algorithm for evolutionary surfaces*, Numerische Mathematik, 58 (1990), pp. 603–  
667 611.
- [17] G. DZIUK AND C. M. ELLIOTT, *Finite element methods for surface pdes*, Acta Numerica,  
669 22 (2013), pp. 289–396, <https://doi.org/10.1017/S0962492913000056>, [http://journals.](http://journals.cambridge.org/article_S0962492913000056)  
670 [cambridge.org/article\\_S0962492913000056](http://journals.cambridge.org/article_S0962492913000056).
- [18] G. FARIN, *Curves and Surfaces for CAGD: A Practical Guide*, The Morgan Kaufmann Series  
672 in Computer Graphics, Academic Press, 5th ed., 2002.
- [19] S. FRAMBATI, H. BARUCQ, H. CALANDRA, AND J. DIAZ, *Practical unstructured splines: Algo-*  
674 *rithms, multi-patch spline spaces, and some applications to numerical analysis*, Journal of  
675 Computational Physics, (2022), p. 111625, [https://doi.org/https://doi.org/10.1016/j.jcp.](https://doi.org/https://doi.org/10.1016/j.jcp.2022.111625)  
676 [2022.111625](https://doi.org/https://doi.org/10.1016/j.jcp.2022.111625), <https://www.sciencedirect.com/science/article/pii/S002199912200688X>.
- [20] R. V. GARIMELLA AND B. K. SWARTZ, *Curvature estimation for unstructured triangulations of*  
678 *surfaces*, tech. report, Los Alamos National Laboratory, 2003.
- [21] T. D. GATZKE AND C. M. GRIMM, *Estimating curvature on triangular meshes*, Inter-  
679 national Journal of Shape Modeling, 12 (2006), pp. 1–28, [https://doi.org/10.1142/](https://doi.org/10.1142/S0218654306000810)  
680 [S0218654306000810](https://doi.org/10.1142/S0218654306000810), <https://doi.org/10.1142/S0218654306000810>, [https://arxiv.org/abs/](https://arxiv.org/abs/https://doi.org/10.1142/S0218654306000810)  
681 <https://doi.org/10.1142/S0218654306000810>.
- [22] E. S. GAWLIK, *High-order approximation of gaussian curvature with regge finite elements*,  
683 SIAM Journal on Numerical Analysis, 58 (2020), pp. 1801–1821, [https://doi.org/10.](https://doi.org/10.1137/19M1255549)  
684 [1137/19M1255549](https://doi.org/10.1137/19M1255549), <https://doi.org/10.1137/19M1255549>, [https://arxiv.org/abs/https://](https://arxiv.org/abs/https://doi.org/10.1137/19M1255549)  
685 [doi.org/10.1137/19M1255549](https://doi.org/10.1137/19M1255549).
- [23] X. D. GU, W. ZENG, F. LUO, AND S.-T. YAU, *Numerical computation of surface conformal*  
688 *mappings*, Computational Methods and Function Theory, 11 (2012), pp. 747–787, <https://doi.org/10.1007/BF03321885>, <https://doi.org/10.1007/BF03321885>.
- [24] C.-J. HEINE, *Isoparametric finite element approximation of curvature on hypersurfaces*,  
690 no. 2004, 26 in Preprint / Mathematische Fakultät, Freiburg, Math. Inst., 2004.
- [25] H. HUANG AND U. ASCHER, *Surface mesh smoothing, regularization, and feature detection*,  
692 SIAM Journal of Scientific Computing, 31 (2008), pp. 74–93, [https://doi.org/10.1137/](https://doi.org/10.1137/060676684)  
693 [060676684](https://doi.org/10.1137/060676684).
- [26] M. LENOIR, *Optimal isoparametric finite elements and error estimates for domains involving*  
695 *curved boundaries*, SIAM Journal of Numerical Analysis, 23 (1986), pp. 562–580.
- [27] L. LI, *Regge finite elements with applications in solid mechanics and relativity*, June 2018.
- [28] Y. LI, *Recovery-based a posteriori error analysis for plate bending problems*, Journal of Sci-  
698 entific Computing, 88 (2021), p. 77, <https://doi.org/10.1007/s10915-021-01595-9>, <https://doi.org/10.1007/s10915-021-01595-9>.
- [29] M. MEYER, M. DESBRUN, P. SCHRÖDER, AND A. H. BARR, *Discrete differential-geometry oper-*  
702 *ators for triangulated 2-manifolds*, in Visualization and Mathematics III, H.-C. Hege and  
703 K. Polthier, eds., Berlin, Heidelberg, 2003, Springer Berlin Heidelberg, pp. 35–57.
- [30] Y. OHTAKE, A. BELYAEV, AND A. PASKO, *Dynamic meshes for accurate polygonization of im-*  
704 *plicit surfaces with sharp features*, in SMI '01: Proceedings of the International Conference  
705 on Shape Modeling & Applications, Washington, DC, USA, 2001, IEEE Computer Society,  
706 p. 74.
- [31] Y. OHTAKE, A. G. BELYAEV, AND I. A. BOGAEVSKI, *Polyhedral surface smoothing with si-*  
708 *multaneous mesh regularization*, Geometric Modeling and Processing, 0 (2000), p. 229,  
709 <https://doi.org/10.1109/GMAP.2000.838255>.
- [32] F. RATHGEBER, D. A. HAM, L. MITCHELL, M. LANGE, F. LUPORINI, A. T. T. MCRAE, G.-  
711 T. BERCEA, G. R. MARKALL, AND P. H. J. KELLY, *Firedrake: Automating the finite*  
712 *element method by composing abstractions*, ACM Trans. Math. Softw., 43 (2016), <https://doi.org/10.1145/2998441>, <https://doi.org/10.1145/2998441>.
- [33] A. RAZDAN AND M. BAE, *Curvature estimation scheme for triangle meshes using biquadratic*  
715 *bézier patches*, Computer-Aided Design, 37 (2005), pp. 1481–1491, <https://doi.org/https://doi.org/10.1016/j.cad.2005.07.001>.

- 717 //doi.org/10.1016/j.cad.2005.03.003, <https://www.sciencedirect.com/science/article/pii/S0010448505000825>.
- 718
- 719 [34] N. S. SAPIDIS, ed., *Designing Fair Curves and Surfaces*, Society for Industrial and Ap-  
 720 plied Mathematics, 1994, <https://doi.org/10.1137/1.9781611971521>, <https://arxiv.org/abs/http://epubs.siam.org/doi/pdf/10.1137/1.9781611971521>.
- 721
- 722 [35] R. SCHNEIDER, L. KOBELT, AND H.-P. SEIDEL, *Mesh fairing based on harmonic mean curva-  
 723 ture surfaces*, in Hierarchical and Geometrical Methods in Scientific Visualization, G. Farin,  
 724 B. Hamann, and H. Hagen, eds., Berlin, Heidelberg, 2003, Springer Berlin Heidelberg,  
 725 pp. 243–267.
- 726 [36] J. SCHÖBERL, *C++11 implementation of finite elements in NGSolve*, Tech. Report ASC-2014-  
 727 30, Institute for Analysis and Scientific Computing, September 2014, <http://www.asc.tuwien.ac.at/~schoeberl/wiki/publications/ngs-cpp11.pdf>.
- 728
- 729 [37] S. W. WALKER, *Tetrahedralization of isosurfaces with guaranteed-quality by edge re-  
 730 arrangement (TIGER)*, SIAM Journal on Scientific Computing, 35 (2013), pp. A294–  
 731 A326, <https://doi.org/10.1137/120866075>, <https://arxiv.org/abs/http://epubs.siam.org/doi/pdf/10.1137/120866075>.
- 732
- 733 [38] S. W. WALKER, *FELICITY: A Matlab/C++ toolbox for developing finite element methods  
 734 and simulation modeling*, SIAM Journal on Scientific Computing, 40 (2018), pp. C234–  
 735 C257, <https://doi.org/10.1137/17M1128745>, <https://doi.org/10.1137/17M1128745>, <https://arxiv.org/abs/https://doi.org/10.1137/17M1128745>.
- 736
- 737 [39] S. W. WALKER, *The Kirchhoff plate equation on surfaces: The surface Hellan-  
 738 Herrmann-Johnson method*, IMA Journal of Numerical Analysis, (2021),  
 739 <https://doi.org/10.1093/imanum/drab062>, <https://doi.org/10.1093/imanum/drab062>,  
 740 <https://arxiv.org/abs/https://academic.oup.com/imanja/advance-article-pdf/doi/10.1093/imanum/drab062/39832913/drab062.pdf>.
- 741
- 742 [40] S. W. WALKER, *Poincaré inequality for a mesh-dependent 2-norm on piecewise linear surfaces  
 743 with boundary*, Computational Methods in Applied Mathematics, 22 (2022), pp. 227–243,  
 744 <https://doi.org/doi:10.1515/cmam-2020-0123>, <https://doi.org/10.1515/cmam-2020-0123>.
- 745
- 746 [41] M. WARDETZKY, M. BERGOU, D. HARMON, D. ZORIN, AND E. GRINSPUN, *Dis-  
 747 crete quadratic curvature energies*, Computer Aided Geometric Design, 24 (2007),  
 748 pp. 499 – 518, <https://doi.org/https://doi.org/10.1016/j.cagd.2007.07.006>, <http://www.sciencedirect.com/science/article/pii/S0167839607000891>. Discrete Differential Geometry.
- 749
- 750 [42] Z. XU AND G. XU, *Discrete schemes for gaussian curvature and their convergence*,  
 751 Computers & Mathematics with Applications, 57 (2009), pp. 1187 – 1195, <https://doi.org/10.1016/j.camwa.2009.01.024>, <http://www.sciencedirect.com/science/article/pii/S0898122109000480>.
- 752
- 753 [43] Z. XU, G. XU, AND J.-G. SUN, *Convergence analysis of discrete differential geometry operators  
 754 over surfaces*, in Mathematics of Surfaces XI, R. Martin, H. Bez, and M. Sabin, eds., Berlin,  
 755 Heidelberg, 2005, Springer Berlin Heidelberg, pp. 448–457.
- 756
- 757 [44] X. YE, T. R. JACKSON, AND N. M. PATRIKALAKIS, *Geometric design of functional surfaces*,  
 758 Computer-Aided Design, 28 (1996), pp. 741 – 752, [https://doi.org/10.1016/0010-4485\(95\)00080-1](https://doi.org/10.1016/0010-4485(95)00080-1), <http://www.sciencedirect.com/science/article/pii/0010448595000801>.
- 759
- 760 [45] X. YIN, M. JIN, F. LUO, AND X. D. GU, *Discrete Curvature Flows for Surfaces and 3-Manifolds*,  
 761 Springer Berlin Heidelberg, Berlin, Heidelberg, 2009, pp. 38–74, [https://doi.org/10.1007/978-3-642-00826-9\\_3](https://doi.org/10.1007/978-3-642-00826-9_3), [https://doi.org/10.1007/978-3-642-00826-9\\_3](https://doi.org/10.1007/978-3-642-00826-9_3).